NAVAL POSTGRADUATE SCHOOL

MONTEREY, CALIFORNIA

THESIS

DEVELOPMENT AND EXPERIMENTAL OPERATION OF A FLASHBOARD PLASMA CATHODE TEST STAND

by

Ali I. Yilmaz

June 2012

Thesis Co-Advisors: John W. Lewellen
John R. Harris

Approved for public release; distribution is unlimited

THIS PAGE INTENTIONALLY LEFT BLANK

REPORT DOCUMENTATION PAGE		Form Approved OMB No. 0704-0188

1. AGENCY USE ONLY *(Leave blank)*	2. REPORT DATE	3. REPORT TYPE AND DATES COVERED
	June 2012	Master's Thesis

4. TITLE AND SUBTITLE Development and Experimental Operation of a Flashboard Plasma Cathode Test Stand	5. FUNDING NUMBERS
6. AUTHOR(S) Ali I. Yilmaz	
7. PERFORMING ORGANIZATION NAME(S) AND ADDRESS(ES) Naval Postgraduate School Monterey, CA 93943-5000	8. PERFORMING ORGANIZATION REPORT NUMBER
9. SPONSORING /MONITORING AGENCY NAME(S) AND ADDRESS(ES) N/A	10. SPONSORING/MONITORING AGENCY REPORT NUMBER

11. SUPPLEMENTARY NOTES The views expressed in this thesis are those of the author and do not reflect the official policy or position of the Department of Defense or the U.S. Government. IRB Protocol number ___N/A____.

12a. DISTRIBUTION / AVAILABILITY STATEMENT	12b. DISTRIBUTION CODE
Approved for public release; distribution is unlimited	

13. ABSTRACT (maximum 200 words)

Flashboard Plasma Cathodes (FBPCs) are potential rugged electron sources for generating high-current beams needed for future High Power Microwave Weapons. In FBPCs, dielectric material is in contact with electrodes in a vacuum. Plasma is generated by a surface flashover discharge on the surface of the dielectric between the electrodes and an electron beam is extracted from the plasma by applying an electric field between the anode and cathode. While FBPCs have been successfully used in a number of applications, the widespread adoption of this technology has been limited by concerns over beam quality. The goals of this thesis are to design a test stand in order to measure FBPC properties that affect beam quality and to enable experiments that will provide a better understanding of the effects of different parameters such as flashboard design, pulser type and plasma properties on the quality of electron beams extracted from the plasma.

14. SUBJECT TERMS	15. NUMBER OF PAGES
Flashboard, Plasma, Cathode, Free Electron Laser, High Power Microwave	81
	16. PRICE CODE

17. SECURITY CLASSIFICATION OF REPORT	18. SECURITY CLASSIFICATION OF THIS PAGE	19. SECURITY CLASSIFICATION OF ABSTRACT	20. LIMITATION OF ABSTRACT
Unclassified	Unclassified	Unclassified	UU

NSN 7540-01-280-5500

Standard Form 298 (Rev. 8-98)
Prescribed by ANSI Std. Z39.18

THIS PAGE INTENTIONALLY LEFT BLANK

Approved for public release; distribution is unlimited

DEVELOPMENT AND EXPERIMENTAL OPERATION OF A FLASHBOARD PLASMA CATHODE TEST STAND

Ali I. Yilmaz
Lieutenant Junior Grade, Turkish Navy
B.S., Turkish Naval Academy, 2006

Submitted in partial fulfillment of the
requirements for the degree of

MASTER OF SCIENCE IN APPLIED PHYSICS

from the

NAVAL POSTGRADUATE SCHOOL
June 2012

Author: Ali I. Yilmaz

Approved by: John W. Lewellen, Ph.D.
Thesis Co-Advisor

John R. Harris, Ph.D.
Thesis Co-Advisor

Andres Larraza, Ph.D.
Chair, Department of Physics

THIS PAGE INTENTIONALLY LEFT BLANK

ABSTRACT

Flashboard Plasma Cathodes (FBPCs) are potential rugged electron sources for generating high-current beams needed for future High Power Microwave Weapons. In FBPCs, dielectric material is in contact with electrodes in a vacuum. Plasma is generated by a surface flashover discharge on the surface of the dielectric between the electrodes and an electron beam is extracted from the plasma by applying an electric field between the anode and cathode. While FBPCs have been successfully used in a number of applications, the widespread adoption of this technology has been limited by concerns over beam quality. The goals of this thesis are to design a test stand in order to measure FBPC properties that affect beam quality and to enable experiments that will provide a better understanding of the effects of different parameters such as flashboard design, pulser type and plasma properties on the quality of electron beams extracted from the plasma.

THIS PAGE INTENTIONALLY LEFT BLANK

TABLE OF CONTENTS

I. INTRODUCTION 1
A. PURPOSE 1
B. BACKGROUND OF HIGH POWER MICROWAVE WEAPONS 2
1. Technical Details and Applications 2
2. Requirements of HPMWs 3
C. BACKGROUND OF CATHODES AND THEIR LIMITATIONS 6
1. Thermionic Cathodes 6
2. Photocathodes 7
3. Secondary Emission 7
4. Field and Explosive Emission (Velvet) Cathodes 8
D. OVERVIEW OF A DIFFERENT CONCEPT: "FLASHBOARD PLASMA CATHODES" 9
1. General Design 9
2. Advantages 12
a. Simple Construction 12
b. Low Sensitivity to Contamination 12
c. Power Saver 12
d. Faster Startup 12
e. Low Cost 13
f. Flexible Control 13
3. Disadvantages and Mitigation Strategies 13
a. Cathode Erosion 14
b. Spatial and Temporal Variation 14
c. Emission Surface Motion 14
d. Plasma Gap Closure 15
e. Emittance Growth 15
4. Summary 16

II. BUILDING A TEST STAND 17
A. FBPC TEST STAND REQUIREMENTS 17
B. VACUUM SYSTEM 18
1. General Requirements 18
2. Turbomolecular Pump 18
3. Ion Pump 19
4. Ion Gauge 20
C. PULSER DESIGN 21
1. Pulsed-Power Supply Requirements 21
2. Pulser Physical Design 22
D. VOLTAGE-CURRENT MONITOR BOX 24
E. FLASHBOARD DESIGN 25
F. LANGMUIR PROBE DESIGN 28
1. What Does a Langmuir Probe Do? 28
2. Initial Langmuir Probe 29

3. Improved Langmuir Probe 30
4. Linear Motion of the Langmuir Probe 30
G. DESIGN OF MESH GRID: "ION STOPPER" 32
1. Overall Design of Ion Stopper 32
2. Ion Stopper Relationship with the Langmuir Probe 33
H. OVERALL DESIGN OF THE FBPC TEST STAND 34
III. EXPERIMENTAL OPERATION AND DATA ANALYSIS 35
A. PULSER OPERATION 35
1. Capacitor Charging 35
2. Capacitor Discharging 36
3. Operation at Higher Charging Voltage 40
4. Mitigation Strategies for the Saturation Effect 44
B. VOLTAGE-CURRENT MONITOR 45
1. General Operation and Design Modifications 45
2. Voltage and Current Monitoring 46
C. FLASHBOARD BREAKDOWN AND PLASMA GENERATION 48
1. Flashboard Breakdown 48
2. Plasma Generation 51
3. Use of Langmuir Probe and Time Delay 52
IV. CONCLUSION AND FUTURE WORK 57
A. SUMMARY 57
B. FUTURE WORK 58
LIST OF REFERENCES 61
INITIAL DISTRIBUTION LIST 65

LIST OF FIGURES

Figure 1. Basic components of a typical electron beam driven HPM system 4
Figure 2. Illustration of a thermionic cathode in an electron gun (From [11]) 6
Figure 3. Photoelectric emission from a cathode surface (After [12]) 7
Figure 4. Secondary emission (From [14]) 8
Figure 5. Basic field emission cathode diagram (From [15]) 8
Figure 6. Microscopic picture of fibers in parallel structure (From [16]) 9
Figure 7. Flashboard seen through the anode grid in a Dielectric Wall Accelerator (From [18]) 10
Figure 8. FBPC basic scheme and expanding plasma 11
Figure 9. Block diagram of the FBPC test stand 17
Figure 10. VARIAN Turbo-V 301-AG turbo pump connected to the test stand 19
Figure 11. VARIAN Star Cell ion pump (left) and its power supply (right) used in the test stand 20
Figure 12. Operation of VARIAN ion gauge inside the vacuum tube in the test stand (left), ion gauge power unit (top right), the whole structure of the ion gauge (bottom right) 21
Figure 13. Circuit diagram of the pulser used in the test stand 22
Figure 14. Physical design of the pulser 23
Figure 15. Pushbutton switch box (left) and MPS 103F ALCO fast-closing switch (right) used for triggering the SCR 24
Figure 16. Voltage-current monitor box (bottom) and its location in the test stand simplified diagram (top) 25
Figure 17. The first surrogate flashboard design 26
Figure 18. The second surrogate flashboard design 27
Figure 19. Full structure of flashboard design (left) and physical version in vacuum chamber (right) 28
Figure 20. A Picture of FBPC and first Langmuir probe used in the test stand 29
Figure 21. New design of the Langmuir Probe 30
Figure 22. Linear shift used in the test stand (From [37]) 31
Figure 23. Linear shift with the ruler gauge 31
Figure 24. A detailed picture of the “ion stopper” 32
Figure 25. A picture of the ion stopper with the Langmuir probe inside the ion stopper 33
Figure 26. Structural relationship between Ion Stopper and Langmuir probe inside the vacuum chamber 33
Figure 27. Final design of the FBPC test stand 34
Figure 28. RLC circuit diagram inside the pulser. Location of Bergoz coils are indicated by “BZ” 35
Figure 29. Charging Voltage Monitor Accuracy 36
Figure 30. Simple RLC circuit model for theory 37
Figure 31. Pulser operation in low voltage in terms of the primary current *without any load* connected to the pulser 38

Figure 32. Pulser operation in low voltage in terms of primary current *with load* connected to the pulser 39
Figure 33. Measured current when charging voltage is 40 Volts *without any load* connected to the pulser 40
Figure 34. Measured currents when charging voltage is 40 Volts *with load* connected to the pulser 41
Figure 35. Measured current when charging voltage is 100 Volts *without any load* connected to the pulser 41
Figure 36. Measured currents when charging voltage is 100 Volts *with load* connected to the pulser 42
Figure 37. Measured currents under applied high voltage..... 43
Figure 38. Bergoz coil and Pearson coil scope traces under 40 V 44
Figure 39. Bergoz coil and Pearson coil scope traces under 100 V 45
Figure 40. V-I Monitor Box circuit diagram (inside the red border). Location of Bergoz (BZ) and Pearson (P) current monitors shown. 46
Figure 41. Measured currents with a simple 28 kΩ load in V-I Monitor Box, and with 100 V pulser operation voltage (no FBPC in this part of the experiment) 47
Figure 42. Measured currents with a simple 28 kΩ load in V-I Monitor Box, and with 300 V pulser operation voltage (no FBPC in this part of the experiment) 47
Figure 43. Measured currents under applied 500 V operational pulser voltage before the FBPC is attached to the circuit 49
Figure 44. Measured currents under applied 500 V operational pulser voltage after the FBPC is attached to the circuit 49
Figure 45. FBPC voltage trace (pink), current trace (yellow), 10x reduced pulser primary current trace (violet) under applied 500 V charging voltage..... 50
Figure 46. First 500 ns period of the break-down process shown by FBPC voltage trace (pink), current trace (yellow), pulser operational current trace (violet) under applied 500 V charging voltage 51
Figure 47. Plasma recognition by using Langmuir probe inside the vacuum chamber after flashboard breaks down 52
Figure 48. One way of using the Langmuir probe to measure plasma velocity (From [13])..... 53
Figure 49. Typical measurement of pulse arrival time to the Langmuir probe 54
Figure 50. Time delay of Plasma..... 55
Figure 51. Distance effect on the plasma time delay. The pink trace is the Langmuir probe plasma signal, the yellow trace is the current of the FBPC, and the violet trace is the 10x reduced primary current. .. 56
Figure 52. Future design of FBPC with anode grid..... 59
Figure 53. Prospective use of multiple Langmuir probes in future experiments (From [13])..... 60

LIST OF ACRONYMS AND ABBREVIATIONS

FBPC	Flashboard Plasma Cathode
FCT	Fast Current Transformer
FEL	Free Electron Laser
HPM	High Power Microwave
HPMW	High Power Microwave Weapon
SCR	Silicon-Controlled Rectifier
UAV	Unmanned Aerial Vehicle
V-I	Voltage-Current

THIS PAGE INTENTIONALLY LEFT BLANK

ACKNOWLEDGEMENTS

I would like to thank Dr. John W. Lewellen and Dr. John R. Harris for their advice and support during my time in their experimental research group at the Naval Postgraduate School (NPS). Their efforts to increase my knowledge brought me to the level where I could easily understand the tough subjects of physics, especially the concept of directed energy weapon systems. I handled the hard work of my technical job in the Beam Physics Laboratory at NPS quickly with the help of their valuable, enjoyable and unforgettable sense of teamwork. The synergy and professional job ethic that they created in the research group motivated me to reach this point of achievement.

I would like to thank my other professors and instructors who taught me and supported me in every aspect of the challenges that I came across in my academic work at NPS.

Finally, I thank my wife, Zeynep, for joining me during my late night studies by keeping me awake and preparing cups of coffee. I appreciate her patience to loneliness while I was away from home and working in the lab.

THIS PAGE INTENTIONALLY LEFT BLANK

I. INTRODUCTION

A. PURPOSE

There is an increasing interest in directed energy weapons based on high power microwave (HPM) technologies. In these systems, electrical energy is converted into microwaves, which carry energy to the target. Potential applications include counter-improvised explosive devices (IEDs) [1], [2], active denial systems [2], and counter-electronics [1], [3]. Although solid-state systems are advancing rapidly, HPM systems still generally rely on electron beam based sources. In general, these sources use an interaction between the electron beam and external circuits and boundaries to bunch the beam at the operating wavelength of the source. When the wavelength is very short, the beam quality must be very good in order to maximize the interaction between the beam and the circuit without losing beam inside the source. However, for longer wavelength sources, the beam quality is less important, and requirements on quality can be relaxed in exchange for high beam current. This suggests the use of flashboard plasma cathodes (FBPCs).

A FBPC consists of a dielectric material in contact with electrodes in a vacuum. Plasma is generated by a surface flashover discharge on the surface of the dielectric between the electrodes and an electron beam is extracted from the plasma by applying an electric field between the anode and the cathode. FBPCs are simple, rugged, inexpensive, and have the potential to generate kilo-ampere-class beams [4]. However, these cathodes have not been widely adopted because of the low beam quality typically associated with them. In addition, expansion of the plasma limits the pulse length of the extracted current from the plasma and can further degrade the beam quality. Consequently, this research is aiming to test FBPCs to understand how to control the plasma properties that affect electron beam quality. This requires construction of a test stand, which is the focus of this thesis.

B. BACKGROUND OF HIGH POWER MICROWAVE WEAPONS

1. Technical Details and Applications

For future military operations, there is an increasing interest in directed energy weapons, including HPMWs. The increasing use of electronic devices in the military, from communication systems to command and control systems, increases the significance of HPMWs in conflicts and threat situations.

HPMWs are systems capable of producing microwaves ranging in frequency from 100 MHz to 300 GHz, and in energy from kilowatts to hundreds of megawatts, and then radiating that energy against a wide range of targets [2]. This energy can cause electronic upset and lethal or non-lethal damage to people and electronic devices by penetrating buildings, vehicles and equipment through very small openings [2], [3].

Since the middle of the twentieth century, militaries around the world have been using electronic devices such as computers, radios, radars, and sonar in every size in operations and combat systems. Today, these electronic devices rely on semi-conductor devices, such as transistors, microchips, and other microelectronic devices, which are highly sensitive to electromagnetic effects. For instance, old style vacuum tube-based systems used high voltages and were relatively large. This meant that a very large electric field would be necessary to upset those systems. Going to semiconductor-based and then microchip-based systems meant that these systems could be much smaller, and needed much less voltage or energy to accomplish their desired job. However, this also makes them much more vulnerable to HPM attacks. Therefore, the increased use of electronic hardware in combat systems represents a tradeoff, in which increased performance is gained at the expense of increased vulnerability to electromagnetic attack. The complexity of electronic systems makes HPMWs able to attack machinery without directly attacking people. Therefore, unnecessary, massive damage and destruction to materials and human beings can be reduced by using HPMWs. It is clear that future battlefields will be full of electromagnetic-based weapons in addition to conventional war instruments such

as bombs, bullets, tanks and troops, which already play a major role in military operations such as defense, anti-terrorism and peace support [1].

There are different kinds of military applications of HPMWs, discussed in previous research, as follows [1]-[3], [5]-[7]:

- Barrier of HPM sources to disrupt low-flying airborne sensors, missiles and platforms (protection of high value targets)
- Reusable Unmanned Aerial Vehicle (UAV)-mounted system for wide-area disruption
- Protection of armored vehicles
- HPM grenades
- Protection of ships in harbor (HPM barrier around ship)
- Speedboat pursuit and disabling
- Barrier of reusable off-board HPM anti-missile systems
- Suppression of enemy air defense
- Aircraft self-protection
- Electronic suppression of communication and security systems
- Neutralization of explosive traps

As a result, future military operations are not expected to require mass destruction, which carries the potential for extensive loss of human life and for violation of human rights. Neutralizing the enemy's electronic equipment will be enough to degrade his ability to fight while reducing the need for massive destruction. HPMWs are, in principle, able to meet these expected requirements whereas kinetic and high explosive weapons do not [1].

2. Requirements of HPMWs

In order to destroy electronic devices via HPM, it is important to concentrate the transmitted energy in a region of the electromagnetic spectrum where the devices are vulnerable. The concern is to produce a high enough electric field at the target, for a long enough time, to achieve the intended change to it. HPM energy can couple into targeted electronic devices through their

antennas, power cables, damaged shielded parts, telephone lines and even holes on shielding cases [3], [5], [6]. To accomplish this, HPMWs need enough peak power to overcome the one-way transit losses (diffraction, absorption, small apertures for entry into target, absorption/protection in target) and still burn out the target hardware.

The overall system needs a power supply, a microwave source, and an antenna. The power source may be batteries or generators, and may include pulsed power stages if needed to produce high-power bursts over short periods. Pulsed power systems will not normally be used with continuous wave systems. Many varieties of microwave sources exist, including magnetron oscillators, klystrons, virtual-cathode oscillators, gyrotrons, free-electron lasers, and beam-plasma generators; all of these convert the kinetic energy of an electron beam into the electromagnetic energy of a microwave beam and generate focused, high-frequency electromagnetic waves [3], [6]. At the end, an antenna points and shoots the HPMs to the target. The antenna has two major functions:

- Impedance match between microwave source and free space
- Gain and directivity (sending the microwaves in a particular direction)

The basic parts of an electron-beam driven HPM system are shown in Figure 1.

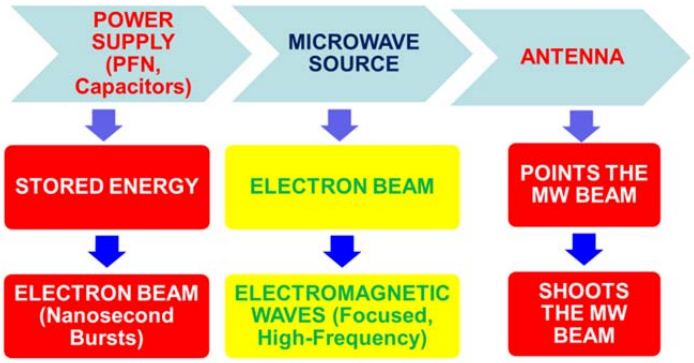

Figure 1. Basic components of a typical electron beam driven HPM system

It is clear in Figure 1 that the critical part of HPMWs is the microwave source, which plays the major role in the system by generating microwaves from the electron beam.

HPM sources can be classified as generators of two major types of microwaves: continuous waves and pulsed waves. FBPCs are not suitable for continuous waves because they are an inherently pulsed device, limited by plasma expansion across the anode-cathode gap and the consequent shorting out of the accelerating field [8]. On the other hand, FBPCs may be suitable for pulsed waves since they use pulsed-power technologies. By generating continuous waves, average powers of tens of kilowatts to megawatts might be achieved [9]. However, peak powers from megawatts to gigawatts can be achieved by using pulsed waves in existing high-power laboratory sources [6].

For several reasons, pulsed weapons are preferable to continuous weapons. It is known that short bursts are more likely than continuous waves to damage electronic hardware and many high power sources can be operated only in the pulsed mode [6]. In addition, pulsed waves would make it harder for the enemy to locate a microwave weapon and take counter measures [6]. Another reason for pulsed systems is to mitigate adverse effects at the antenna: the air around the antenna might turn into plasma because of the high power, which would interfere with the microwave propagation [3]. This effect also sets a constraint on the design of the antenna, even for short pulse systems. For instance, if the HPM propagation is focused too tightly, the peak electric field may be high enough to ionize the air.

The need for pulsed, high-current electron beams to generate intense microwaves motivates the desire for improved electron sources. This includes FBPCs, which might be a better approach for HPMWs than other cathodes currently in use.

C. BACKGROUND OF CATHODES AND THEIR LIMITATIONS

Cathodes are devices used for producing free electrons. By the early 1900s, it was known that electrons are bound to matter. The valence electrons in metals are “free”—they are able to move easily from atom to atom. However, they are not able to leave the surface of the material easily and escape into vacuum. Several electron emission methods are known and these methods determine the type of cathodes available today. Some cathode types have been in use for many years and some are still under investigation. The types of cathodes in widespread use can be grouped into four different categories according to their emission methods and their limitations for possible use in HPM systems.

1. Thermionic Cathodes

This type of cathode is based on thermionic emission, in which an application of heat allows electrons to gain enough energy to escape from the material [10]. Figure 2 shows the basic elements of a thermionic cathode.

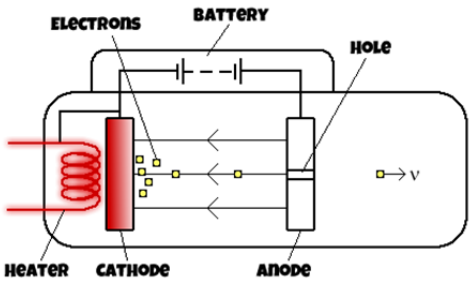

Figure 2. Illustration of a thermionic cathode in an electron gun (From [11])

For many applications requiring high-current pulsed electron sources, thermionic cathodes cannot produce sufficient current density. In addition to this, some thermal stress problems may occur due to the heater element. Temperature variation across the cathode surface leading to variation in the emission current density is another related problem. Some materials used in the

cathode surface to achieve high temperature, low work function surfaces may cause contamination of the electron gun.

Another limitation of thermionic cathodes is that they are inherently CW electron sources. The thermal mass of the cathode prevents its temperature from being pulsed rapidly. So, emission must be gated by applying pulsed electric fields, typically by using grids. These complicate pulsed operation, degrade beam quality, and may intercept the beam.

2. Photocathodes

The principle of photocathode operation depends on the photoelectric effect, which consists of incident light shining on the material and transferring energy to the electrons [10]. As a result, this energy transfer allows electrons to escape from the material. Figure 3 demonstrates the photoemission process.

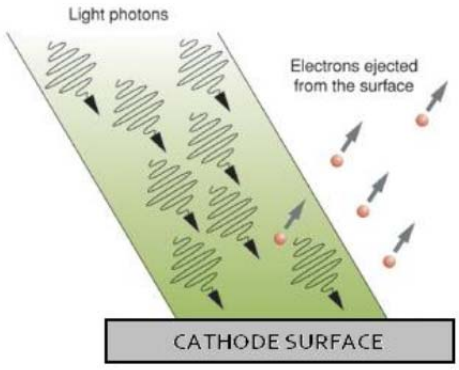

Figure 3. Photoelectric emission from a cathode surface (After [12])

Photocathodes are the electron sources of choice for Free Electron Lasers (FELs), but are not suitable for future, very high current HPM systems, because the laser required to drive very high currents would be too expensive [13].

3. Secondary Emission

The main idea behind the secondary emission process is the electron bombardment of the cathode material as shown in Figure 4. The electrons in the

surface of the cathode material gain energy from the incident high-speed electrons or other particles. The secondary electrons are liberated from the surface.

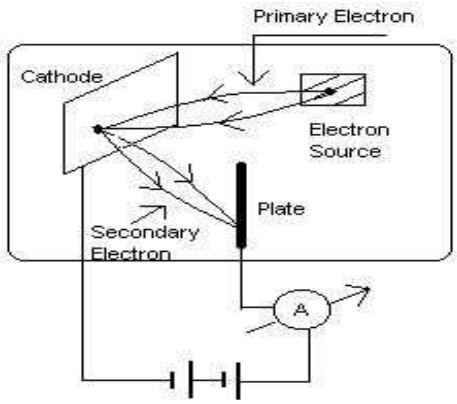

Figure 4. Secondary emission (From [14])

This emission type is not usually used as an electron source for HPM systems because it requires a primary electron current and depends on the preparation of the surface of the cathode material, which decreases flexibility and increases the system cost.

4. Field and Explosive Emission (Velvet) Cathodes

In traditional field emission cathodes, a strong electric field allows the valence electrons to escape from the cathode material. This type of cathode requires very high electric fields. Figure 5 shows one implementation of a field emission cathode.

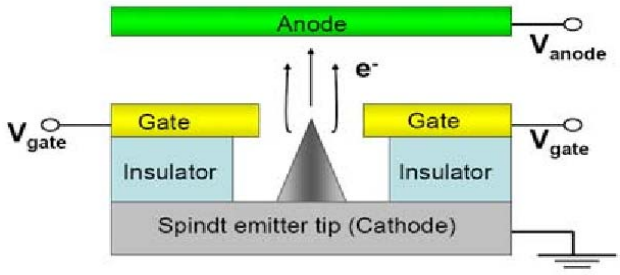

Figure 5. Basic field emission cathode diagram (From [15])

In explosive electron emission cathodes, electric fields do not necessarily need to be as high as for simple field emission. Explosive electron emission usually implies a source such as a velvet cathode. Velvet cathodes use arrays of fibers as in Figure 6, oriented parallel to the applied electric field. Electrons produced by field emission at field enhancement sites strike the fiber, and produce secondary electrons. This process generates plasma along the fiber, and that plasma can then emit electrons due to the applied field.

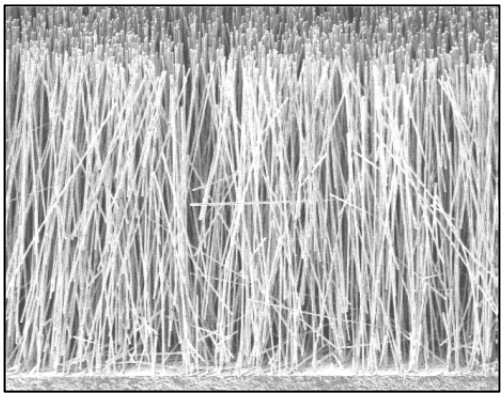

Figure 6. Microscopic picture of fibers in parallel structure (From [16])

Although many HPM sources use explosive electron emission cathodes [17], they are not able to decouple the plasma generation process from the beam extraction process because the same electric field that generates the plasma also extracts the electron beam from that plasma. Separating these processes provides additional flexibility in controlling the system and is one of the main advantages of FBPCs.

D. OVERVIEW OF A DIFFERENT CONCEPT: "FLASHBOARD PLASMA CATHODES"

1. General Design

Typical flashboards consist of a large number of contacts in an array on a dielectric surface as shown in Figure 7.

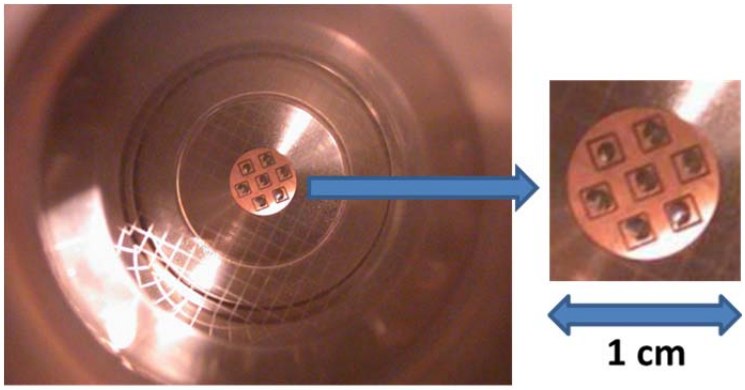

Figure 7. Flashboard seen through the anode grid in a Dielectric Wall Accelerator (From [18])

When high voltage is applied across the electrodes, there will be a discharge across the gap between these electrodes. This discharge causes a surface flashover, which generates expanding plasma over the flashboard.

Flashboards have been widely used in many experiments in different laboratories. They have been used to generate plasmas as the basis of plasma cathodes [8], [18]-[22], and also in plasma opening switches [23]-[28] and in microwave tubes as plasma sources [29]. Plasmas generated by flashboards have been investigated and found to consist mostly of protons and carbon ions [30].

When used as the basis for FBPCs, the flashboard is first used to generate plasma, and then by using a separate pulsed beam extraction voltage, electrons can be extracted from the plasma. By separating the plasma formation process from the beam extraction process, the device becomes more flexible than other pulsed plasma cathodes such as explosive emission cathodes.

A basic scheme of an intended physical design of a FBPC is shown in Figure 8.

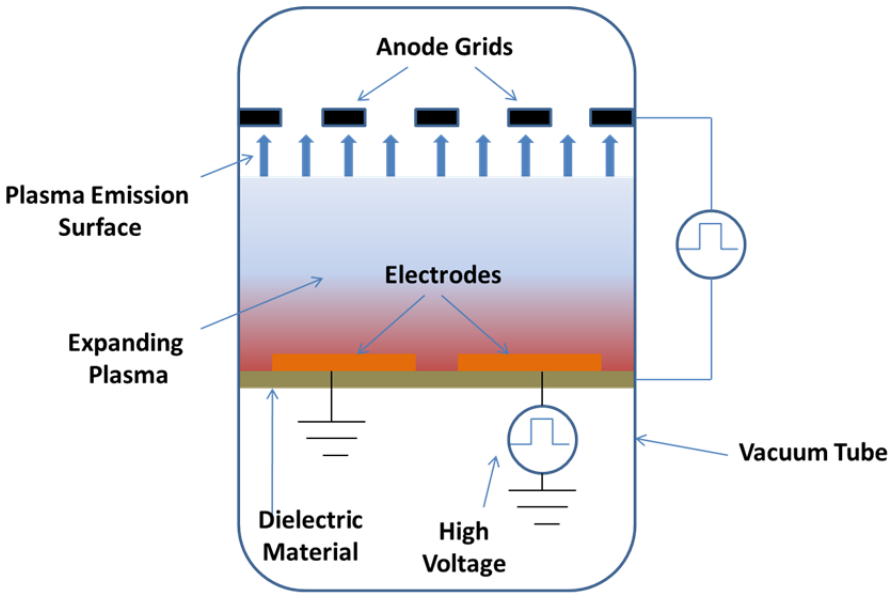

Figure 8. FBPC basic scheme and expanding plasma

Cathodes generating plasma for use as electron sources have been under investigation by researchers since the 1970s [8], [18], [31]-[33]. S. Humphries and his colleagues at the University of New Mexico worked on the plasma cathode to show its potential applications to the generation of pulsed-electron beams using a grid-controlled system [31]. J.R. Bayless and his group developed a new type of plasma cathode electron gun qualified for pulsed and continuous wave operation with electron beam lasers [32]. J.R. Harris and his colleagues at Lawrence Livermore National Laboratory developed a short-pulsed dielectric wall accelerator using a surface flashover plasma cathode as shown in Figure 7 [18]. S.E. Sampayan and S.H. Gurbaxani investigated the properties of vacuum gap closure, including plasma initiation, its movement toward the anode, and the emission of electrons from the plasma in a plasma cathode, in their research at the University of New Mexico [8]. In addition, Ady Hershcovitch at Brookhaven National Laboratory also used a plasma cathode as a source of super thermal electrons in an electron gun [33].

2. Advantages

a. Simple Construction

FBPCs are simple to design and there are no complicated or sophisticated parts among their basic components. They operate at room temperature so that thermal stress, which can cause problems in a thermionic source, is eliminated. In addition, there is no need to cool down the FBPC to very low temperatures in order to have it operate efficiently.

b. Low Sensitivity to Contamination

While FBPCs are not sensitive to contamination, there is no absolute isolation of contamination for them as well. The discharge process can actually be aided by surface contamination. The plasma produced by the FBPCs is likely to contain many different chemicals. Over time, the flashboard material will be eroded away by the discharges, and these can contaminate other parts of the system. However, even in conventional thermionic emission sources, work function lower in chemical substances coming off the cathode surface can result in contamination of the system.

c. Power Saver

Some cathodes, such as thermionic cathodes, need a continuous supply of power. On the other hand, FBPCs require power only for a few microseconds or less, which comprises the discharge period across the electrodes. FBPCs use this intermittent power for a very short time so that it reduces the average power need for operating the FBPC.

d. Faster Startup

FBPCs do not require any warm-up or stand-by period and produce plasma immediately after the high voltage discharge occurs on the flashboard. A weapon system may be required to become ready to attack a target in as small a

period as 3 or 5 seconds. Therefore, the short period of time required for starting up a weapon system using a FBPC is a major advantage for this technology.

e. Low Cost

Because of the simplicity of the parts used in their design, FBPCs are relatively cost-efficient electron sources. The materials chosen to build the FBPC are inexpensive and found easily in the market.

f. Flexible Control

There are two major processes in creating high current electron beam from a plasma cathode: plasma generation and beam generation from the plasma. These two processes are combined in other types of pulsed plasma cathodes such as explosive electron emission cathodes in which a high electric field causes not only the plasma generation from the cathode material but also the beam generation. Separating these two functions provides improved control and flexibility of the FBPC by allowing independent adjustment of flashover voltage, pulse length, extraction voltage, and timing. However, this does require multiple power sources (DC or pulsed-power) to generate electric fields separately for the plasma formation and electron extraction.

3. Disadvantages and Mitigation Strategies

A number of disadvantages to FBPCs have been reported in the literature, including possible erosion of the cathode, spatial and temporal variations of the plasma emission surface and its motion, plasma gap closure limiting the pulse length, current variation during beam generation, and relatively high emittance [8], [33], [34]. Some of these disadvantages are inherent in the way FBPCs operate and impose constraints on their use, while others may be corrected with improved designs.

a. Cathode Erosion

Over time, the flashboard material will be eroded away by repeated discharges. This will tend to widen the gaps, increasing the voltage needed to initiate a discharge. In addition, the material removed from the flashboard may contaminate other parts of the system resulting a reduced lifetime for them as well. However, not all experiments with flashboards show major erosion. A flashboard tested by J. R. Harris and his colleagues showed only minor discoloration in the gap after one-year of intermittent operation totaling 500 shots [18]. Minimizing the energy put into the plasma, minimizing the duration of the pulse and perhaps alternate material selection may lead to a better design with reduced erosion.

b. Spatial and Temporal Variation

Spatial and temporal variations in the plasma produced by FBPCs were previously reported by Lawrence Livermore National Laboratory. In those tests, when the plasma cathode discharged, higher and lower density regions were observed in the plasma, leading to high- and low-current regions in the beam [35]. The pattern of these variations changed from shot-to-shot, and led to increased emittance. Biasing resistors and improved gap geometries may mitigate these shot-to-shot variations in the pulse as suggested in Ref. [18].

c. Emission Surface Motion

The complexity of the shape and motion of the plasma surface makes calculations difficult. If the surface expansion occurred in a simple planar fashion as shown in Figure 8, this would make the theory of plasma movement simpler. But in reality, identifying the shape of the emission surface is more complicated, making it more difficult to define the actual problem geometry. In addition, the shape will change over time, and will affect the initial trajectories of the electrons. For instance, if the plasma conductivity is high enough that it can be treated like a conductor, electric field lines will be perpendicular to the plasma surface as shown in Figure 8. If the plasma shape—its curvature—changes as it

expands, the electric field lines will also change depending on that curvature. As a result, the electron beam initial conditions as well as beam current will change as the plasma moves across the gap.

d. Plasma Gap Closure

In general, systems using FBPCs have a gap between the flashboard and the anode. After plasma is generated over the flashboard, it will expand through the gap. Depending upon on the expansion velocity of the generated plasma, plasma will close the gap and make a short circuit between the cathode material and the anode in a relatively short time. When the plasma occupies the vacuum gap, the electron extraction process will stop.

Figure 8 demonstrates the plasma expansion through the vacuum gap. Earlier researchers carried out experiments investigating how to slow down the plasma expansion velocity [8], [24], [31]. The expansion velocity ranges from 1 to 30 cm/μs [8], [19], [22]-[28], [30], [35].

e. Emittance Growth

Emittance is a measure of how tightly the electron beam can be focused. Generally, the smaller the wavelength of electromagnetic radiation that a system is producing, the more tightly focused the electron beam must be. For example, in an x-ray FEL (short wavelengths), the optical mode tends to be small so efficient coupling between electron beam and the optical mode requires very small emittance. On the other hand, IR FELs (longer wavelengths) tend to have larger optical modes so that they do not require as small an emittance as an x-ray FEL. Since its wavelength is even larger, the emittance can be even bigger for a HPM source.

Since FBPCs have a reputation for high emittance, they may not be well suited for FELs. Instead, they are likely to be better suited for pulsed HPM sources. In FBPCs, it may be possible to reduce the emittance of the electron beams they produce by improving the FBPC design and electron extraction

process. The separation of the plasma generation and beam extraction processes may help mitigate this problem.

4. Summary

FBPCs offer a number of advantages for pulsed HPMWs, such as simplicity, low sensitivity to contamination, reduced power consumption, fast startup, low cost and flexible control of the plasma and beam generation processes. Their disadvantages, including cathode erosion, spatial and temporal variation, complexity of emission surface motion, anode-cathode gap closure of plasma and high emittance, are less problematic when used for pulsed HPMWs than for other applications. Remaining issues to improve and study include designing a flashboard, generating plasma and electron beam by using pulsed power, controlling the plasma surface emission, measuring the plasma velocity and electron extraction voltage, measuring the other plasma properties such as plasma temperature and plasma density. Before these issues can be studied, a suitable test stand must be constructed to allow for characterization of the plasma produced by FBPCs. This will be the focus of the remainder of this thesis.

II. BUILDING A TEST STAND

A. FBPC TEST STAND REQUIREMENTS

This test stand is expected to provide enough observation of the operation of FBPCs so that the research group can begin to do experiments to improve the understanding of FBPC operation and optimization.

This test stand requires a reasonably low pressure relative to atmosphere. The FBPC operates under vacuum, and requires low pressures ($< 10^{-6}$ Torr) which can be achieved with vacuum pumps and pressure gauges which are in common use. Another requirement is a pulser, which generates a high voltage pulse and transfers the energy from a DC power source to the FBPC in order to break down the spark gap and cause a surface flashover, which is the mechanism for plasma generation. In order to diagnose the plasma and its expansion in vacuum, a Langmuir probe can be used. As a final stage in the test stand, different types of diagnostic instruments are required, such as an oscilloscope to study waveforms, as well as voltage and current monitors to measure power delivered to the FBPC. A diagram of the entire FBPC test stand is illustrated in Figure 9.

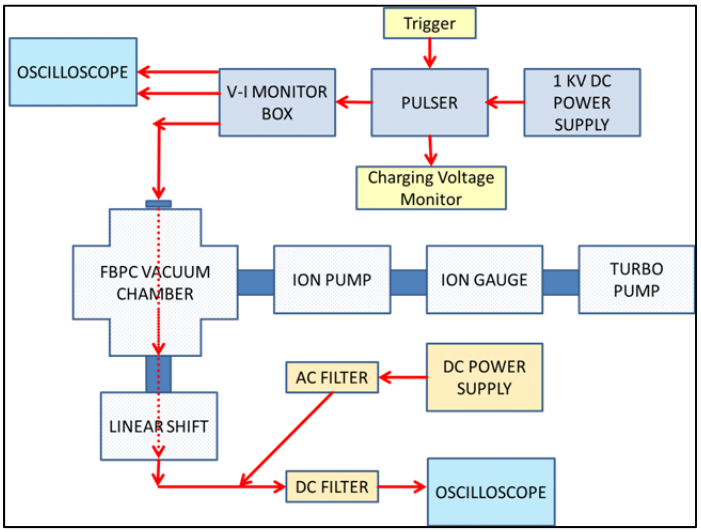

Figure 9. Block diagram of the FBPC test stand

B. VACUUM SYSTEM

1. General Requirements

Because FBPCs are intended to produce electron beams in vacuum, both the FBPCs and test stand materials must be compatible with vacuum. Vacuum pressures of 10^{-6} Torr or better are required for FBPCs, compared to 10^{-8} -10^{-10} Torr for most accelerator systems.

2. Turbomolecular Pump

The choice of which vacuum pump to use in a system depends primarily on the size of the experimental test stand volume and the desired base pressure. Turbomolecular pumps are one of these pump choices and are one of the better options for use in systems that are small in volume such as this FBPC test stand. A turbomolecular pump consists of movable and fixed blades in a turbine configuration. This turbine rotates very fast, deflecting gas molecules from inlet port to the outlet port, thereby creating a pressure gradient and allowing it to create or maintain vacuum. When used with a suitable roughing pump, turbo pumps can operate from atmospheric pressure down to very low pressures such as 10^{-8} Torr. On the other hand, there are some disadvantages: if the power fails, it will vent the system to air. In addition, moving parts wear out over time and can be damaged by debris impacting the blades.

For this test stand, the VARIAN Turbo-V 301-AG turbomolecular pump shown in Figure 10 is used for initial pump down from atmospheric pressure. It is a user friendly, computer-based pump, which has a long lifetime and instantaneous start-up. While the vacuum inside the vacuum chamber in the test stand reaches about 10^{-6} Torr in the first five minutes, it takes almost four days to reach 10^{-7} Torr.

Figure 10. VARIAN Turbo-V 301-AG turbo pump connected to the test stand

3. Ion Pump

Ion pumps are another option for pumping systems to very low pressures such as 10 orders of magnitude smaller than atmospheric pressure. When gas molecules enter the ion pump, the pump ionizes and accelerates them with voltages of typically 3 kV to 7 kV, and traps them using a magnetic field perpendicular to the electric field. The ions impact titanium plates, where they are trapped by chemical reactions or are physically buried in the plates, depending on the gas species.

The VARIAN Star-Cell ion pump and power supply used in this test stand are shown in Figure 11. This pump provides a measured base pressure of 10^{-8} Torr. When pumping down, the vacuum inside the test stand reaches about 10^{-6} Torr in the first five minutes by using turbomolecular pump, with the ion pump bringing down the pressure to 10^{-8} Torr in about three minutes. It keeps this pressure as long as it stays on.

Figure 11. VARIAN Star Cell ion pump (left) and its power supply (right) used in the test stand

4. Ion Gauge

Both the turbo pump (located approximately one meter away from the flashboard chamber) and the ion pump (located right before the flashboard chamber entrance) measure the pressure inside their own chambers. In order to sort between these two different measurements at different locations in the pumping system, an ion gauge, which is even closer to the flashboard, is used to take alternative vacuum pressure measurements for comparison.

The whole structure of the VARIAN ion gauge with the control unit is shown in Figure 12. Thermionic emission generates electrons from the filament, which bombards the gas inside the tube, causing ion generation. These ions are collected by the thin wire at the center of the wire cage in Figure 12, causing a current, which depends on the pressure inside the vacuum chamber. The measured pressure is typically an order of magnitude greater than the pressure measured by the ion pump itself.

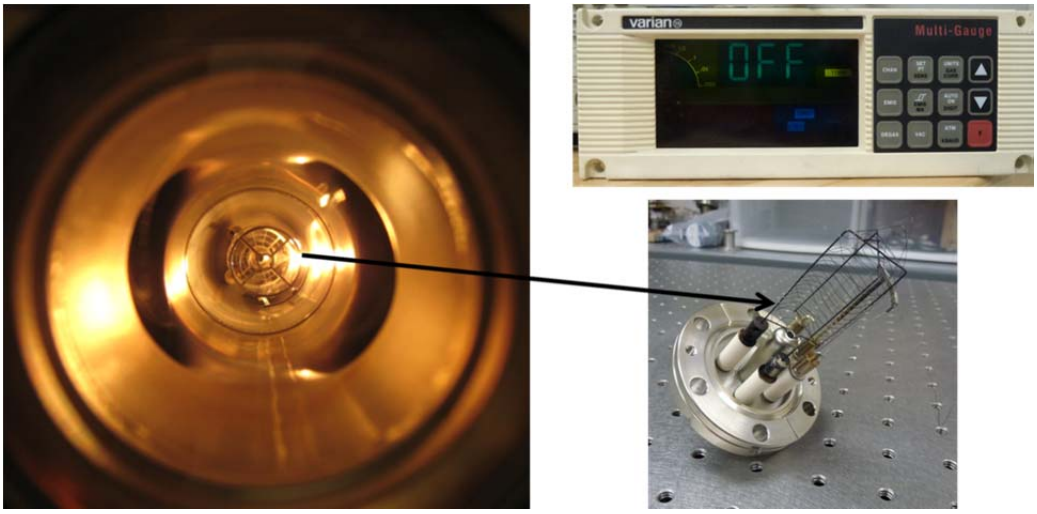

Figure 12. Operation of VARIAN ion gauge inside the vacuum tube in the test stand (left), ion gauge power unit (top right), the whole structure of the ion gauge (bottom right)

C. PULSER DESIGN

1. Pulsed-Power Supply Requirements

In order to produce a discharge to activate the FBPC, this test stand needs to produce a high enough voltage to break down the FBPC gap. Once this has happened and plasma has been produced, high voltage is no longer needed; but enough current is still required to sustain the discharge for long enough to produce the plasma. Putting too much energy into the plasma will heat it, and possibly increase its expansion velocity, which may increase the emittance of a beam that the FBPC would produce. Initially, the voltage, current, and pulse length that the system required were unknown. In addition, this test stand is limited to 5 kV and no beam extraction because of the radiation safety limitations under which this test stand is currently operating.

The pulser built for initial operation of this test stand consists of an LRC circuit switched by a Silicon-Controlled Rectifier (SCR) generating a voltage applied across a step-up transformer.

Since the pulsed-power supply provides a single short pulse, it provides the opportunity, when used with fast diagnostics, to study the details of the

system's operation on a relatively fast timescale. A DC source or a CW source providing many continuous pulses at the same level would not provide the same ability to understand what is happening.

2. Pulser Physical Design

A circuit diagram of the pulser is provided in Figure 13.

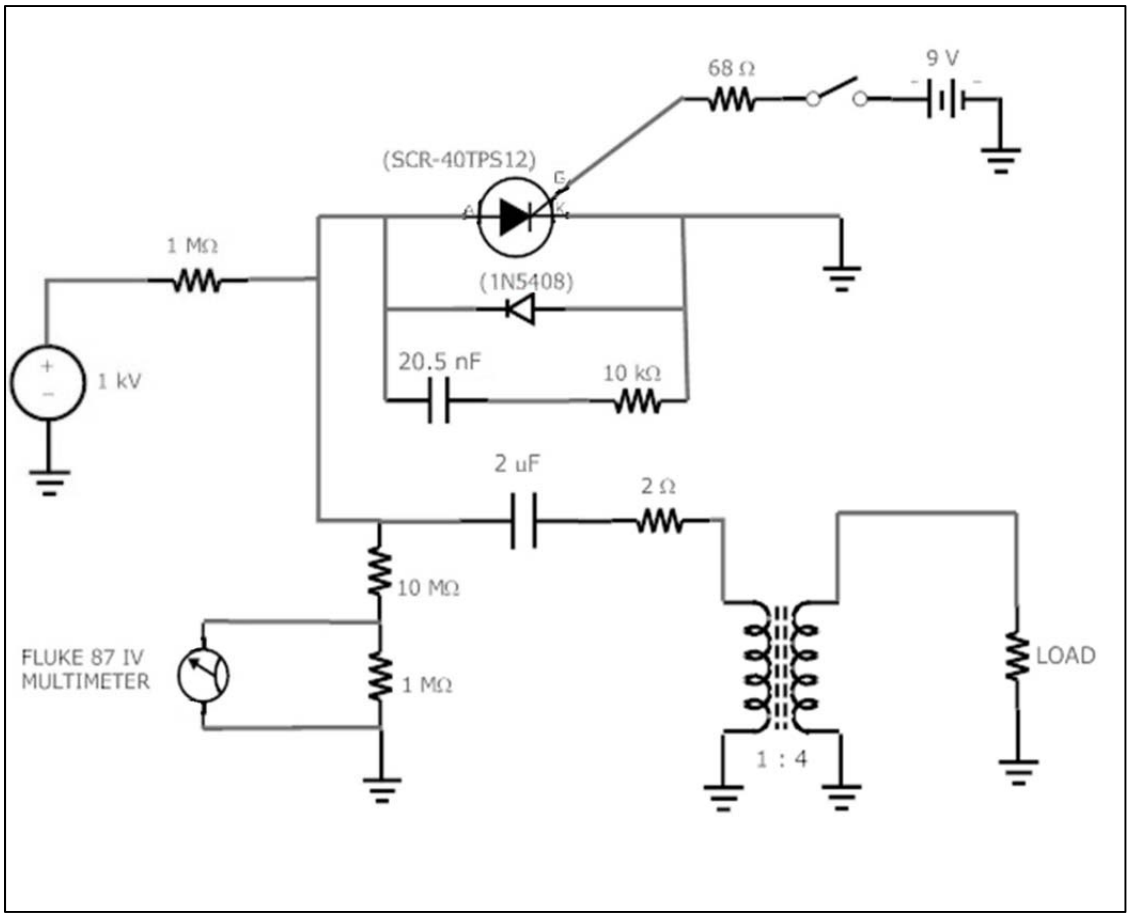

Figure 13. Circuit diagram of the pulser used in the test stand

The load shown in Figure 13 is a resistor, but could either the FBPC spark gap or other loads used for testing. The pulser designed for the present experimental work and the charging voltage meter are shown in Figure 14.

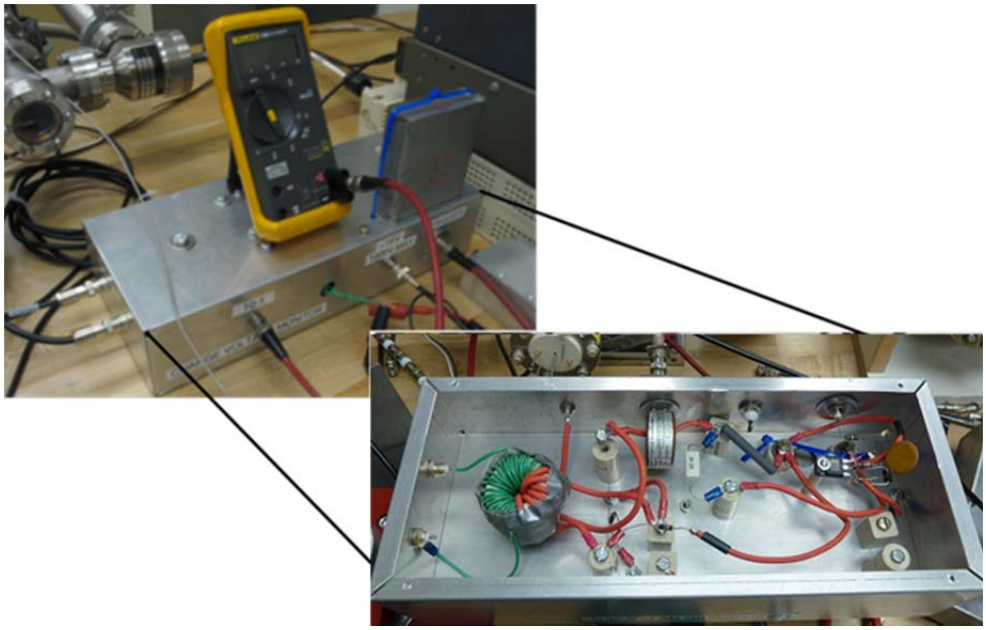

Figure 14. Physical design of the pulser

In order to obtain a maximum 5 kV output voltage, the pulser uses a capacitor, which has a nominal capacitance of 2.0 μF and a measured capacitance of 2.17 μF, and that can be charged up to 1.2 kV (limited by the SCR). A 40TPS12 model SCR was used in the pulser. SCRs are designed for medium power switching and phase control applications. When the gate-cathode voltage exceeds a certain threshold value (1.45 V for this SCR), the SCR turns on and conducts current. Triggering, in other words “switching,” is a one-time process with a certain switching speed; the switching speed for this SCR is 1000 V/μs and 100 A/μs. A pushbutton switch (MPS 103F ALCO), shown in Figure 15, was used for triggering the SCR. It is housed in a small box containing a simple circuit hosting a 9.0 V industrial battery that provides enough voltage turn on the SCR.

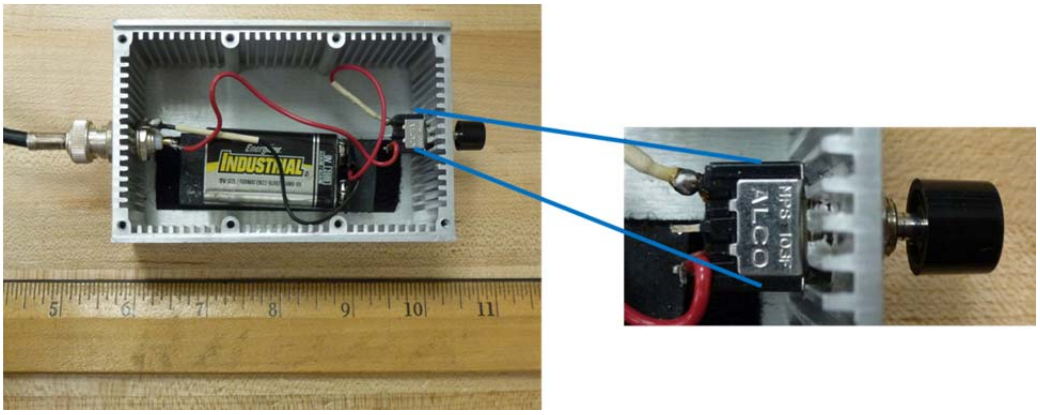

Figure 15. Pushbutton switch box (left) and MPS 103F ALCO fast-closing switch (right) used for triggering the SCR

D. VOLTAGE-CURRENT MONITOR BOX

Measuring the voltage and the current across the flashboard during operation provides a measure of the power that the pulser puts into the plasma. Therefore, the voltage-current monitor box takes power measurements at any time during the 'on-period' of the pulser. Its photograph and location in the test stand diagram are shown in Figure 16.

As illustrated in Figure 16, voltage-current monitoring occurs in a metal box with two Bergoz fast current transformers (FCTs). These are passive devices optimized for non-contact measurements of fast current pulses, with rise times faster than 1 ns and a sensitivity of 1.25 V/A. Inside the FCT, there are wire turns around an alloy core, and a 50Ω load. When non-contact primary current passes through the center of the FCT core, a proportional signal is generated and can be viewed on an oscilloscope [36]. In this test stand, one of the FCTs measures the current flowing through the FBPC, while the other measures the voltage across a grounded resistor that is parallel to the flashboard and therefore gives the same voltage applied across the flashboard during the pulse.

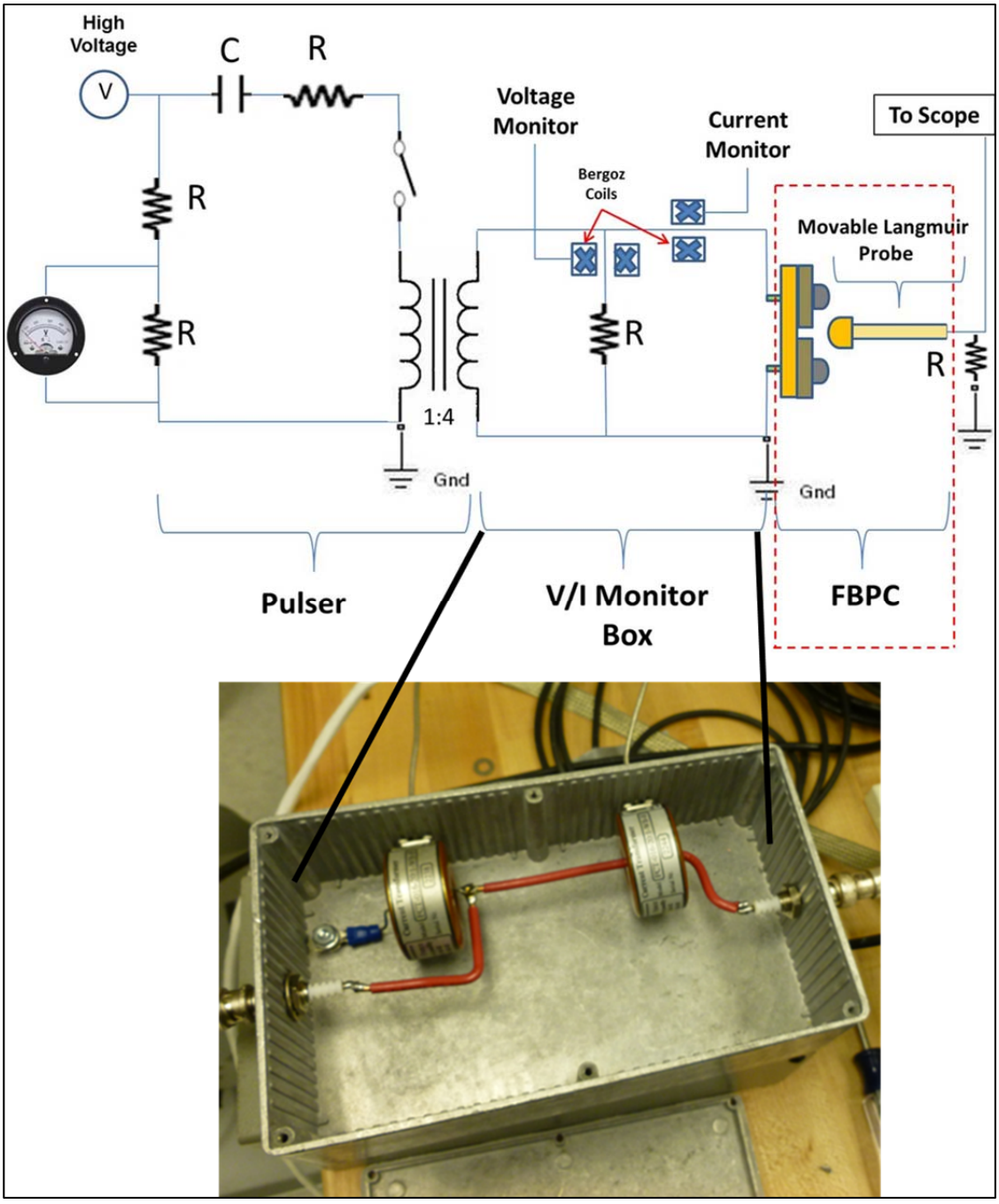

Figure 16. Voltage-current monitor box (bottom) and its location in the test stand simplified diagram (top)

E. FLASHBOARD DESIGN

In general, a flashboard consists of both dielectric material and conductive electrodes. Virtually any dielectric or conductor can be made into a simple

flashboard, although the choice of materials will influence the lifetime and operating properties of the flashboard, and the nature of the contamination it produces.

This design used PVC as the dielectric surface and aluminum tape as the conductor, both of which are inexpensive and easy to handle, and can be easily found in the market.

After deciding on the materials, this work aimed to find an acceptable design for the surrogate flashboard that operates, in other words, can be broken down by the applied high voltage pulse, under almost every pressure from atmosphere to very low pressures such as 10^{-8} Torr or 10^{-9} Torr. For simplicity of initial testing, a single gap was used rather than the array of gaps normally used, as shown in Figure 7.

The first flashboard design consisted of a dielectric material and electrodes, which are in contact with the dielectric material. There was a space between these electrodes of approximately a few tenths of a millimeter, in order to form a spark gap. To provide a field enhancement to assist the breakdown process, the inner edges of the electrodes facing each other are pointed. In addition to assisting the breakdown process, this should help localize the discharge to the same point during every shot. Figure 17 illustrates the final drawing of the first design.

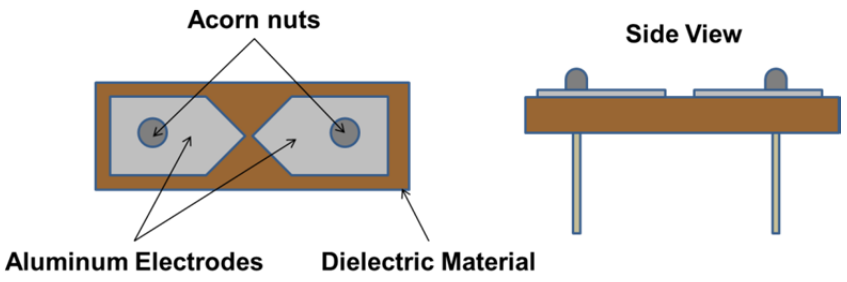

Figure 17. The first surrogate flashboard design

The first design was prone to damage because of the difficulty in making the cross cut at the center of the electrodes without removing too much material

from the dielectric. This knife-cut style made the spark gap too big so that larger voltages were required, and any damage to this area caused the FBPC not to break down at voltages less than about 1 kV pulser charging voltage.

A second surrogate flashboard was designed, in which the electrodes were changed as illustrated in Figure 18. This design only requires one straight cut, which is easier to make while keeping the gap small and the edges sharp.

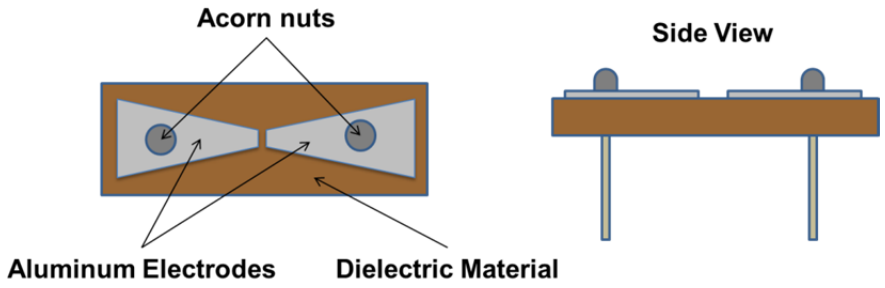

Figure 18. The second surrogate flashboard design

This provided a gap of a few tenths of a millimeter, which fixed the prior problem and allowed the spark gap to break down with low charging voltages of 160–170 V.

During the first high voltage operation of the surrogate flashboard in Figure 18, a short occurred between the electrode rods and the vacuum chamber. After insulating the rods with tygon tubing as shown in Figure 19, this problem was solved and the surrogate flashboard discharged as expected.

Note that brass rods were used in the current transmission system in the vacuum chamber although using brass in a high vacuum system is generally not recommended due to its high vapor pressure. Its use was acceptable in this system because while ultra-high vacuum (< 10^{-9} Torr) was not required, brass is strong enough to keep the flashboard straight without deflection and is easily shaped.

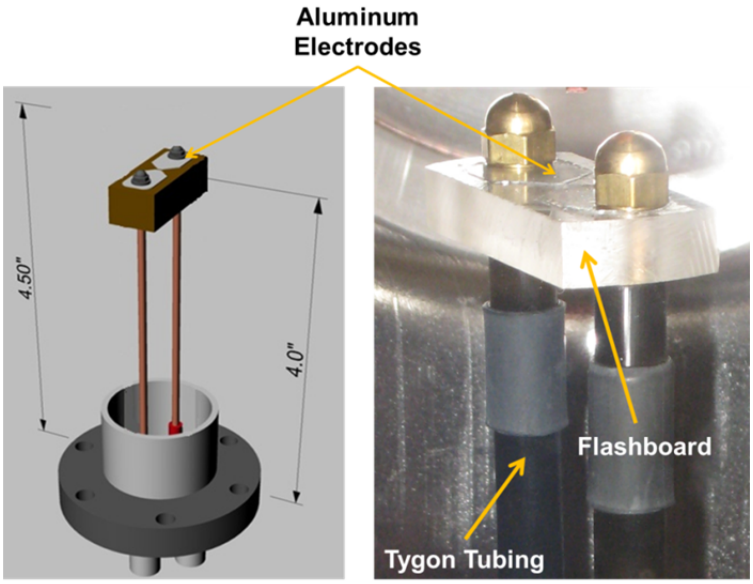

Figure 19. Full structure of flashboard design (left) and physical version in vacuum chamber (right)

F. LANGMUIR PROBE DESIGN

1. What Does a Langmuir Probe Do?

A Langmuir Probe is composed of an exposed conductor, like a wire, immersed within the plasma and is used to diagnose the properties of the plasma such as plasma potential, electron density, ion density, electron temperature, and plasma velocity. While Langmuir probe techniques can be very sophisticated, in the initial experiments reported here, these probes were used as simple indicators of the presence or absence of plasma.

Because of the design of this test stand, there is nothing constraining the plasma to be stationary. Instead, plasma generated during FBPC operation will move away from the flashboard, with typical expansion speeds reported in the literature ranging from 1 to 30 cm/μs [8], [19], [22]-[28], [30], [35]. Because of this, the Langmuir probe in this experiment can be used for answering questions such as: Is the plasma there or not? What is the time of plasma arrival? What is the net charge of the particles in the plasma (as shown by positive or negative scope traces)? What is the energy of the particles in the plasma (by taking

biased probe measurements)? Finding answers to these questions will provide a better understanding of the plasma movement and may lead to methods to mitigate the effects of emission surface motion on the extracted electron beam properties.

2. Initial Langmuir Probe

The initial Langmuir probe had two conductors, consisting of copper wires. These wires were insulated except at the tips, while the other ends of the wires were connected to the feedthrough pins at the flange. Two wires were used in an attempt to measure conduction through the plasma. However, while they did not seem to measure any conduction, they did give some idea about the arrival time of the pulsed plasma when connected to the scope. A picture of the first Langmuir probe is shown in Figure 20. In order to provide sufficient mechanical rigidity, wire ties were used to keep the two wires together; however, this Langmuir probe still had insufficient mechanical rigidity.

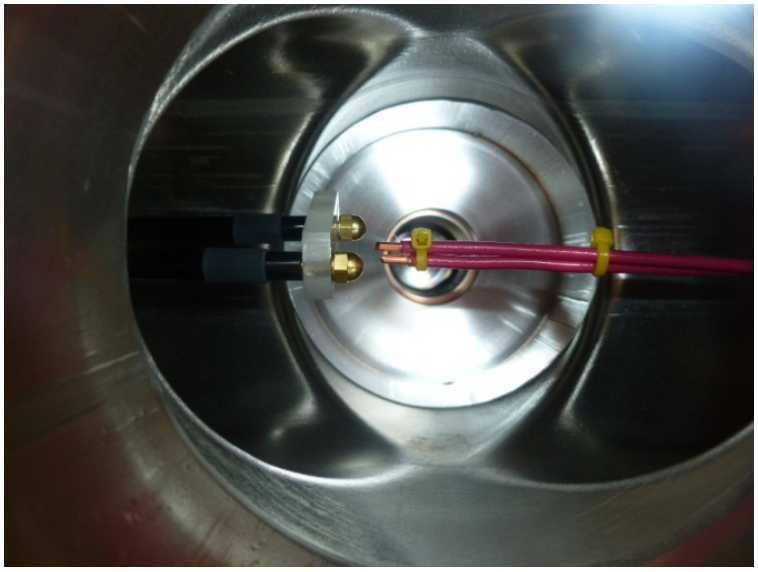

Figure 20. A Picture of FBPC and first Langmuir probe used in the test stand

3. Improved Langmuir Probe

An improved probe was designed from scratch, and is shown in Figure 21. The new probe is a rigid 12 inch-long brass rod, 2 mm in diameter. An acorn nut is used to make the surface area of the tip larger than the previous one (enlarged from 1 mm to 5 mm in diameter) to sample more of the plasma. The outer surface of the probe must be insulated so that only plasma striking the tip will create a signal. In order to insulate the probe, tygon tubing was used as seen in Figure 21 (yellow insulator around the probe).

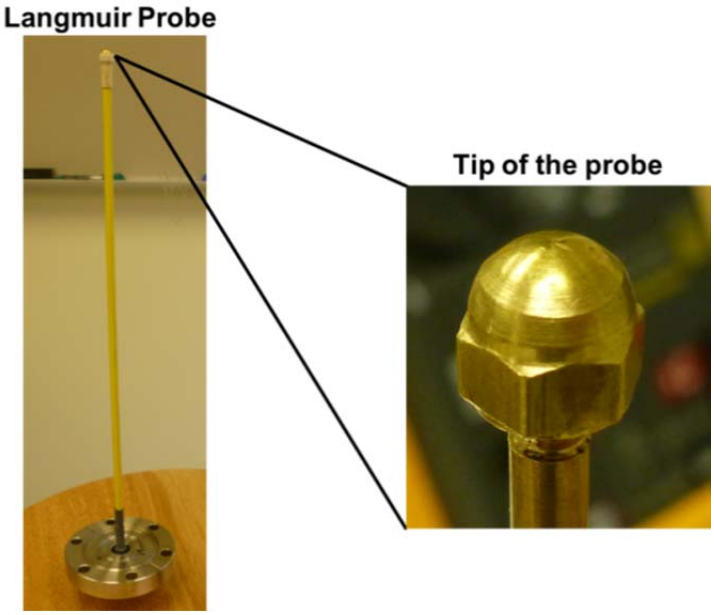

Figure 21. New design of the Langmuir Probe

4. Linear Motion of the Langmuir Probe

The Langmuir probe in this test stand is not a fixed probe, but it moves back and forth by means of the linear shift, a picture of which is shown in Figure 22.

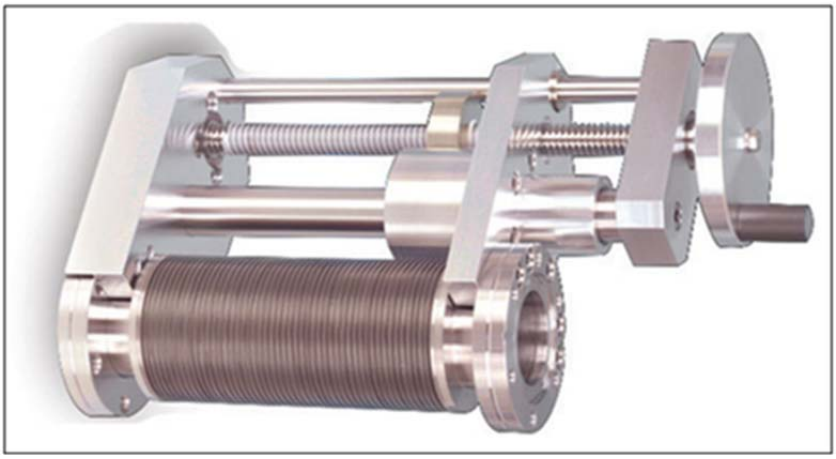

Figure 22. Linear shift used in the test stand (From [37])

The Langmuir Probe is connected directly to the linear shift so that the distance between the flashboard and the probe can be adjustable. It is also possible to take exact measurements of Langmuir probe distance from the flashboard in the vacuum chamber by mounting a precision dial gauge. A final structure of the linear shift with the dial gauge is shown in Figure 23.

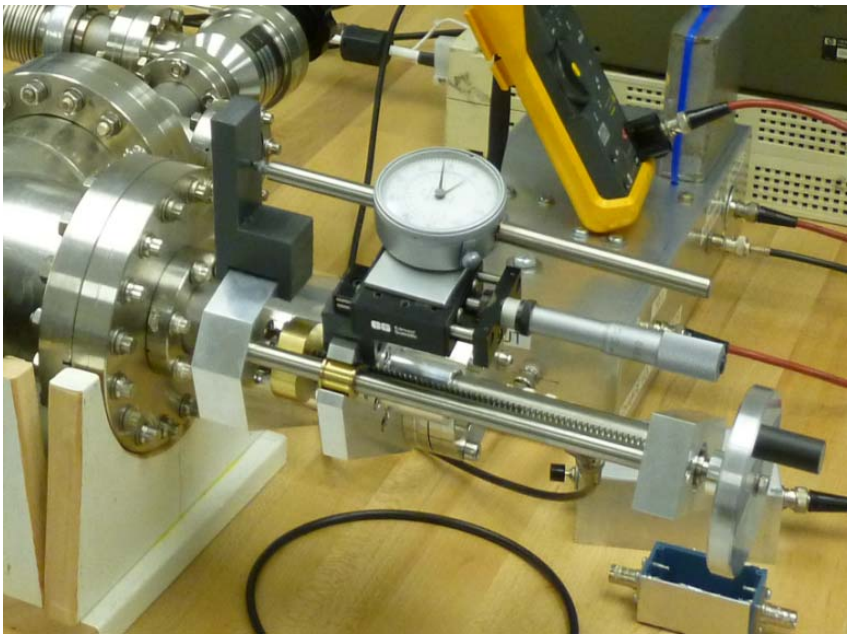

Figure 23. Linear shift with the dial gauge

G. DESIGN OF MESH GRID: "ION STOPPER"

1. Overall Design of Ion Stopper

In order to distinguish between electron and positive ion currents in the Langmuir probe signals, a mesh grid with a long cylinder metal sheet of 1 mm thickness, called an "ion stopper" was built as seen in Figure 24.

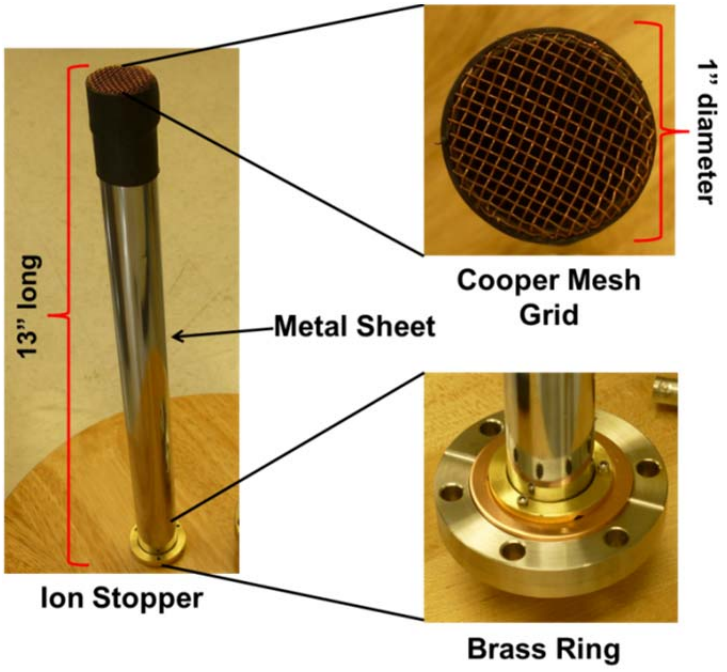

Figure 24. A detailed picture of the "ion stopper"

The main idea behind this design is to set up an electric field between the grid and the Langmuir probe to help control what type of particles are able to reach the probe. This operation occurs when the copper mesh grid is connected to the base flange with the help of a metal sheet that, at the same time, covers the Langmuir probe and grounds the grid. There is no electrical contact between the ion stopper and the Langmuir probe. The evolution of the ion stopper around the Langmuir probe is pictured in Figure 25.

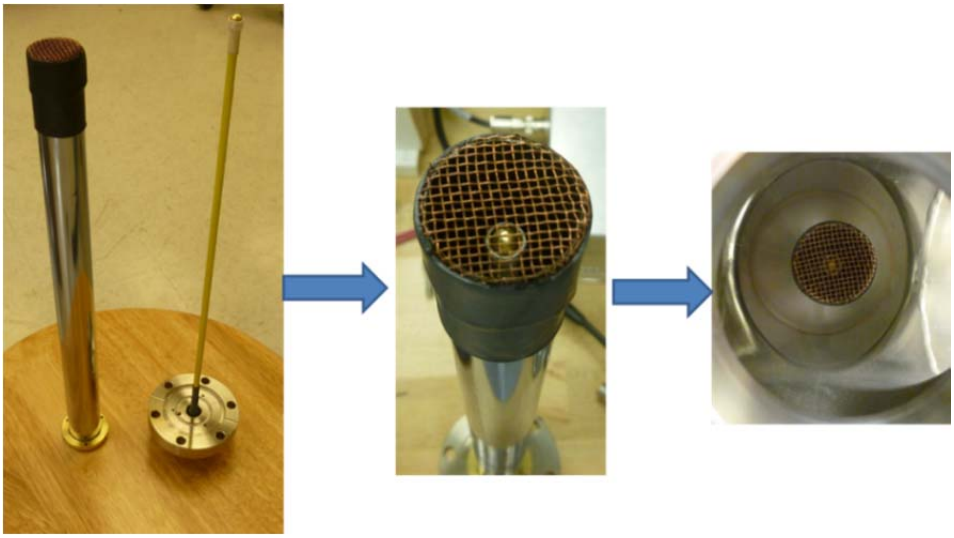

Figure 25. A picture of the ion stopper with the Langmuir probe inside the ion stopper

2. Ion Stopper Relationship with the Langmuir Probe

The ion stopper is mounted around the Langmuir Probe as in Figure 25. There is no physical connection between the Langmuir Probe and the ion stopper structure. Figure 26 explicitly illustrates the connections of the different parts on the same diagram.

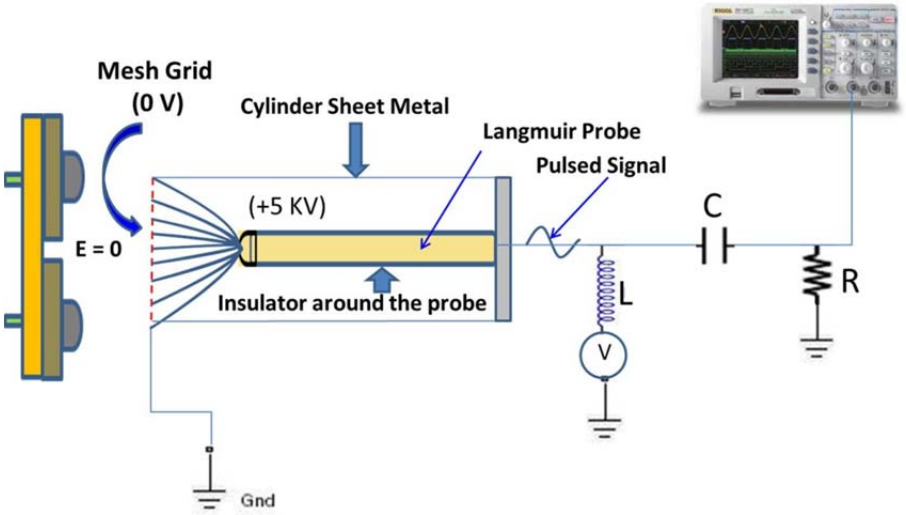

Figure 26. Structural relationship between Ion Stopper and Langmuir probe inside the vacuum chamber

In Figure 26, an external DC voltage (up to 5 kV) is applied to the probe through an inductor, which behaves as a short under DC currents. Since the mesh grid attached to the cylinder sheet metal is grounded, an electric field occurs between the mesh grid and the tip of the Langmuir probe. However, the electric field is still zero in front of the flashboard. The electric field between the mesh and the probe can be tuned by changing the DC voltage, and acts as a separator that separates electrons from the other charged particles so that the electron and positive ion components of the plasma can be investigated clearly. On the other hand, the capacitor in Figure 26 works as an isolator. While it allows the pulsed signal to pass from the Langmuir probe to the oscilloscope, it also protects the oscilloscope from DC voltage by behaving as an open at DC.

H. OVERALL DESIGN OF THE FBPC TEST STAND

The final design of the test stand is pictured in Figure 27. This picture is consistent with the entire diagram shown in Figure 9.

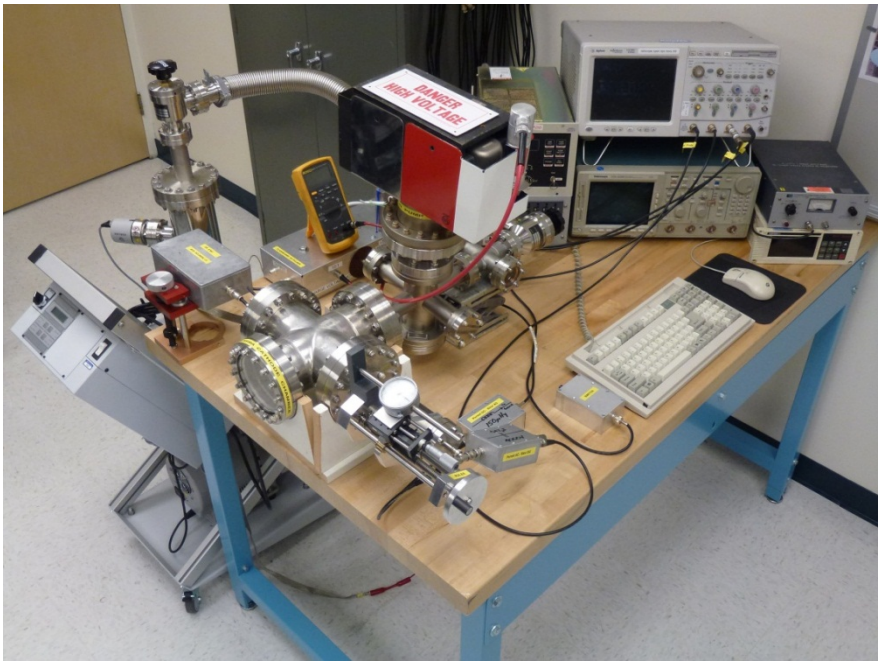

Figure 27. Final design of the FBPC test stand

III. EXPERIMENTAL OPERATION AND DATA ANALYSIS

A. PULSER OPERATION

1. Capacitor Charging

Figure 28 shows the pulser as configured for testing. At the heart of this system is the main energy storage capacitor. Before the test stand can operate, this capacitor must be charged to the desired operating voltage. This is accomplished by an external Hewlett-Packard HARRISON 6515A DC power supply (0-1600 V) connected to the capacitor through a 1.0 MΩ resistor, which protects the power supply from excessive current during pulser operation. The maximum operational charging voltage is 1.2 kV, which is set by the voltage rating of the SCR. In normal operation, the charging voltage is monitored using a resistive voltage divider consisting of a 1.0 MΩ resistor and a 10.0 MΩ resistor in series (actual values 1.0 MΩ and 9.9 MΩ), with voltage read across the smaller resistor using a Fluke multimeter.

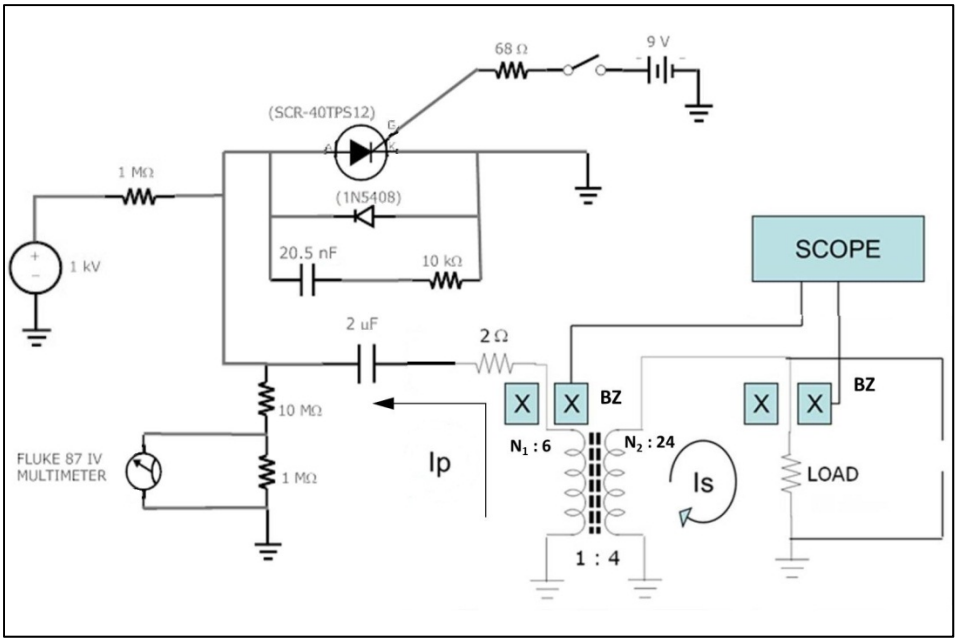

Figure 28. RLC circuit diagram inside the pulser. Location of Bergoz coils are indicated by “BZ”

Figure 29 shows calibration data comparing the voltage across the smaller resistor to the voltage measured directly across the capacitor terminals using a second Fluke multimeter. The voltage divider response is very linear, and well approximated by the theoretical voltage division ratio based on the resistors' nominal values.

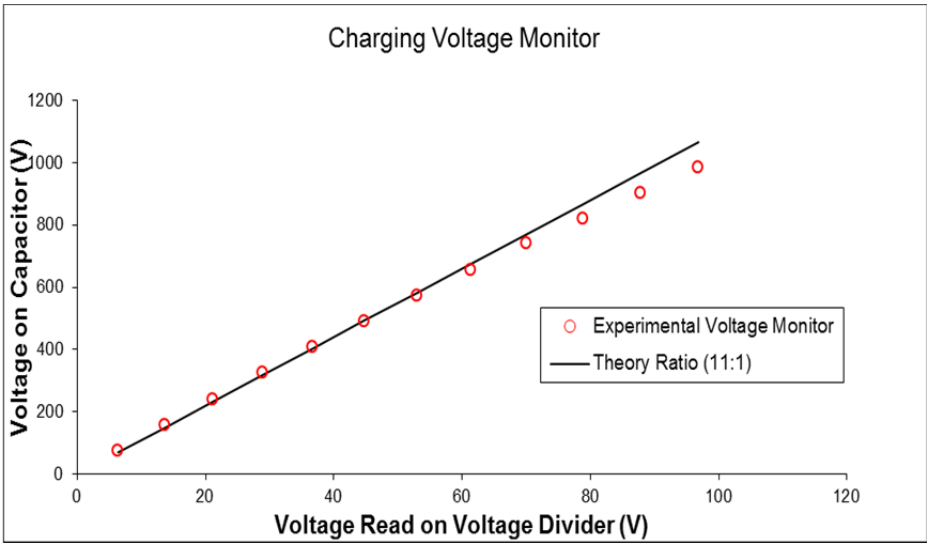

Figure 29. Charging Voltage Monitor Accuracy

2. Capacitor Discharging

After the capacitor is charged, the pulser may be activated by depressing the firing button, which triggers the SCR. The capacitor then discharges through the SCR, producing a current I_p in the primary winding of the transformer, and a current I_s through the secondary winding and load if a load is attached.

After the SCR begins to conduct, the pulser can be modeled with a simple RLC circuit, as shown in Figure 30.

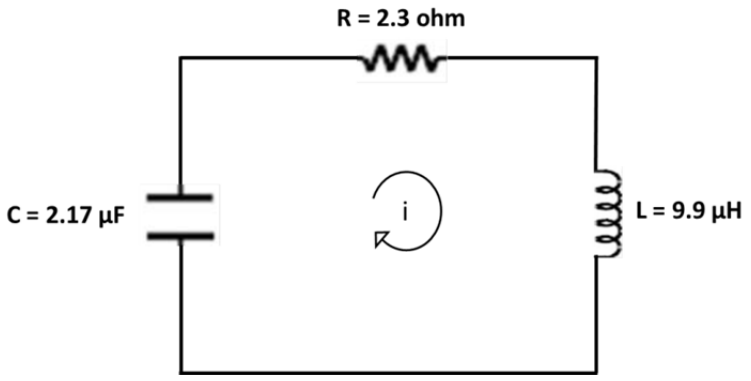

Figure 30. Simple RLC circuit model for theory

The current i flowing in this circuit is governed by the differential equation

$$\frac{d^2i}{dt^2} + \frac{R}{L}\frac{di}{dt} + \frac{1}{LC}i = 0 \ , \qquad (1)$$

where R, L and C are the measured values from the actual circuit, as shown in Figure 30. Because of these values, the circuit will be under-damped, and the solution to Equation 1 is

$$i(t) = Ae^{-\frac{R}{2L}t}\cos(\omega t) + Be^{-\frac{R}{2L}t}\sin(\omega t) \ , \qquad (2)$$

where ω is

$$\omega = \sqrt{\frac{1}{LC} - (\frac{R}{2L})^2} \ . \qquad (3)$$

After applying the initial condition $i(t=0)=0$ to this equation, one of the constants is found: $A=0$. As a result, Equation 2 becomes

$$i(t) = Be^{-\frac{R}{2L}t}\sin(\omega t) \ . \qquad (4)$$

As soon as the switch closes, since the initial current is zero, the voltage drop across the resistor will also be zero. So the charging voltage V_{ch} on the capacitor must equal the voltage across the inductor, so

$$V_{ch} = -L\frac{di}{dt} \quad at \;\; t = 0. \tag{5}$$

From Equation 4,

$$\frac{di}{dt} = B\frac{R}{2L}e^{-\frac{R}{2L}t}\sin(\omega t) - Be^{-\frac{R}{2L}t}\,\omega\cos(\omega t) \tag{6}$$

is obtained. After the initial condition in Equation 5 is applied for t, the constant becomes $B = -CV_{ch}\omega$. Therefore,

$$i(t) = -CV_{ch}\omega\, e^{-\frac{R}{2L}t}\sin(\omega t) \tag{7}$$

Equation 7 describes the primary side of the circuit, without any load connected across the secondary. Figure 31 shows a comparison between the theoretical current predicted by Equation 7 and the experimental current initially measured at a low charging voltage, and without any load connected to the pulser.

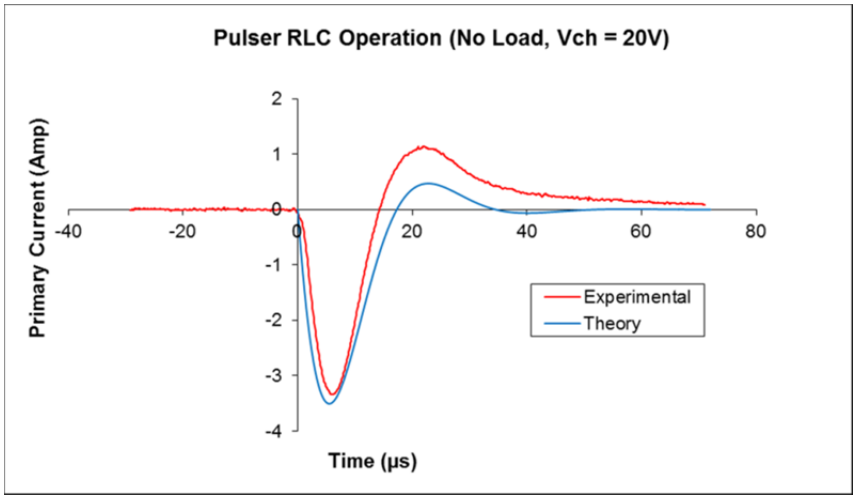

Figure 31. Pulser operation in low voltage in terms of the primary current *without any load* connected to the pulser

The experimental data was collected by use of the Bergoz coil, mounted into the primary side of the transformer, as shown in Figure 29.

Figure 32 shows the pulser primary and secondary currents when a load was connected to the secondary side.

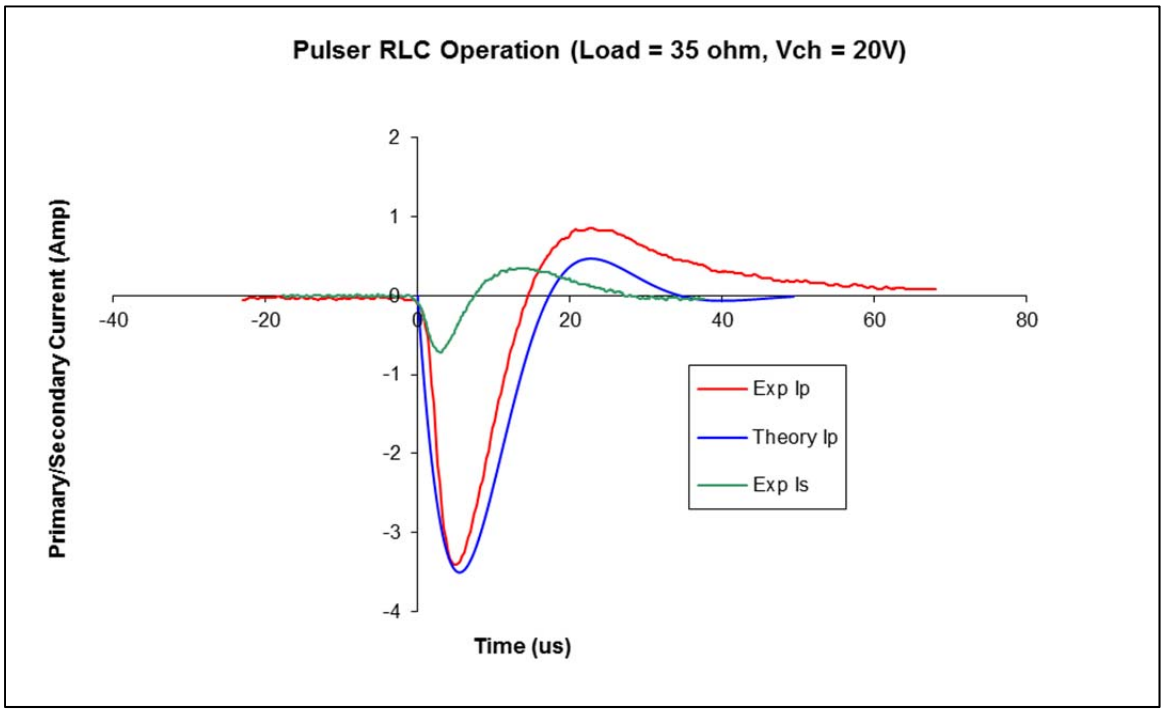

Figure 32. Pulser operation in low voltage in terms of primary current *with load* connected to the pulser

While the pulser was no longer the simple RLC circuit shown in Figure 30, the primary current was relatively unchanged from the prediction of Equation 7. Figure 32 also shows the current through the secondary, measured with a Bergoz FCT. In this case, a 35 Ω load was connected in parallel with the secondary. The Bergoz coil was being used to measure the current through that resistor – effectively giving a measure of the voltage applied across the secondary, which in turn will be proportional to the voltage across the primary, which in turn should be proportional to the derivative with respect to time of the current through the primary. Figure 32 shows that this is the case.

3. Operation at Higher Charging Voltage

At very low charging voltages, the primary current measured by the Bergoz coil agreed very well with the theoretical prediction for a simple RLC circuit. However, as the charging voltage was increased, the measured primary current no longer agreed with the theory. Figure 33 illustrates how the measured primary current distorts when the charging voltage is increased up to 40 V, near the onset of this effect.

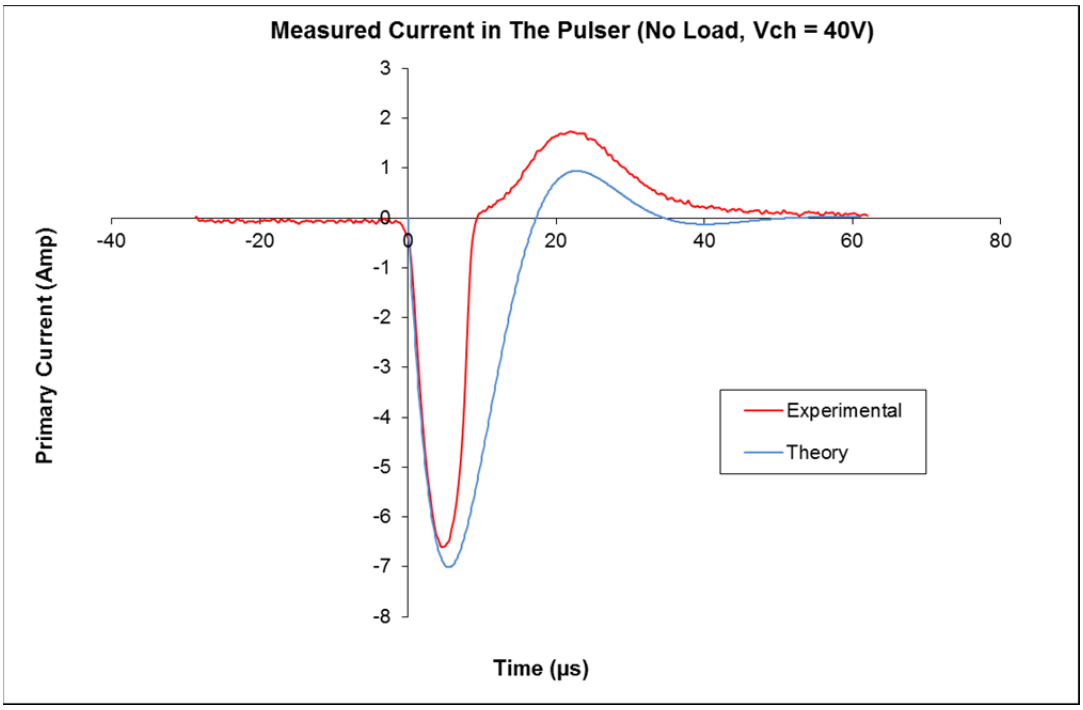

Figure 33. Measured current when charging voltage is 40 Volts *without any load* connected to the pulser

The primary current trace in Figure 33 and in Figure 34 follows the theory curve up to almost 7.0 A. However, it peaks at a slightly lower value than the theory curve predicts, and drops down to 0 A earlier than expected from the theory.

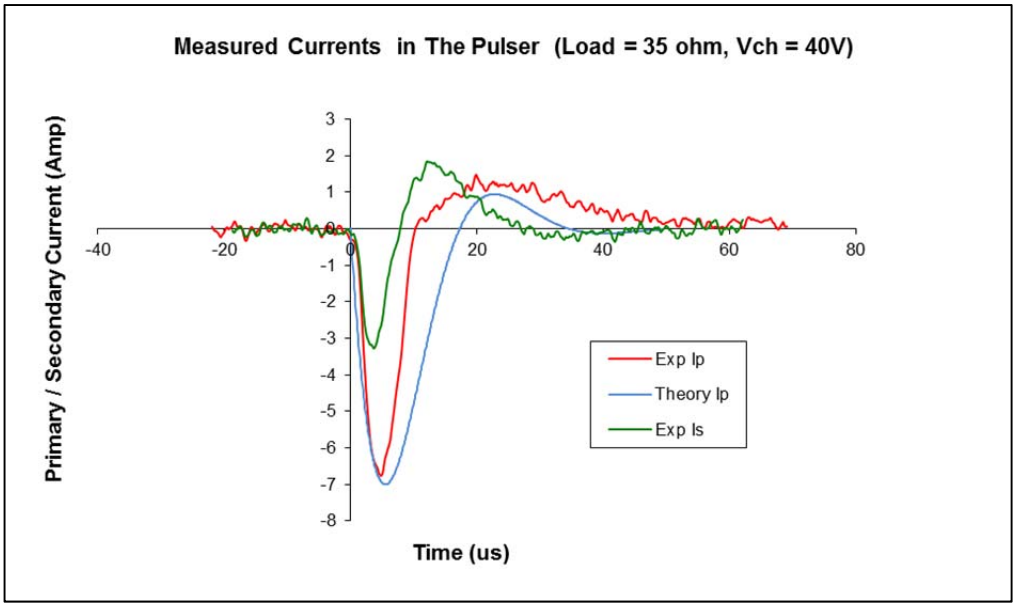

Figure 34. Measured currents when charging voltage is 40 Volts *with load* connected to the pulser

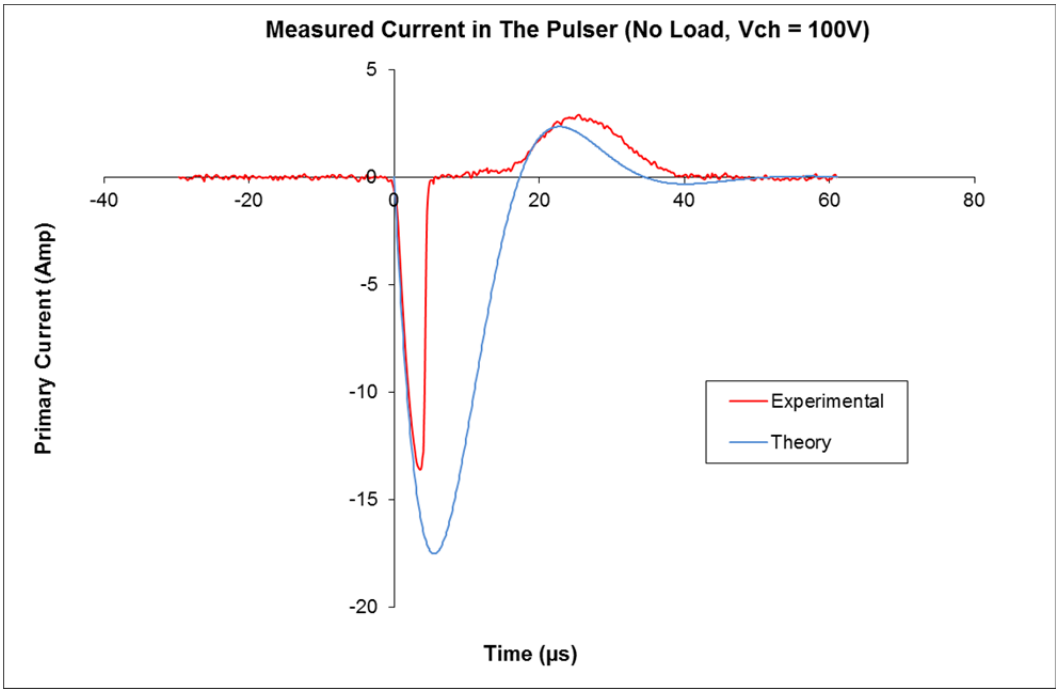

Figure 35. Measured current when charging voltage is 100 Volts *without any load* connected to the pulser

In Figure 35, as the charging voltage was increased up to 100 V, the effect becomes more noticeable. Figure 36 illustrates operation at the same charging voltage, but with a load connected to the pulser.

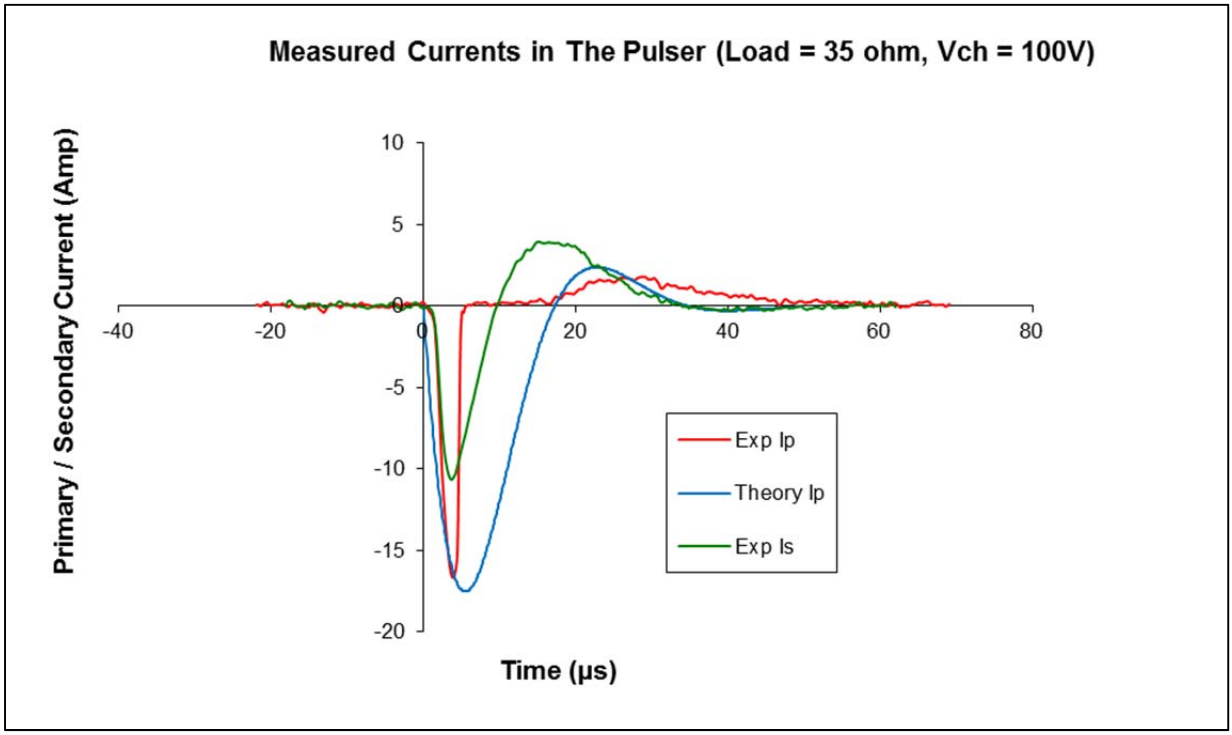

Figure 36. Measured currents when charging voltage is 100 Volts *with load* connected to the pulser

To sum up, at 20 V in Figure 31 and Figure 32, the effect starts at the end of the pulse. As the voltage is increased, the effect occurs before the pulse reaches its theoretical peak value, so most of the pulse is "chopped off" and thrown away, and just a little bit of the pulse from the leading edge of the theoretical pulse is seen as shown in Figure 35 and Figure 36. Notice that the shape of the measured secondary current traces seems unchanged.

As the charging voltage increased, the area under the first part of the primary current curve appeared to be constant after a certain point. This is similar to behavior seen in pulsed power systems when a pulse transformer's "volt-second" product is exceeded and it goes into saturation. Ferromagnetic core

materials cannot provide infinite magnetic flux densities, and when the applied current through the primary side exceeds the point at which all the magnetic domains in the core align, the transformer saturates. When this happens, the relative permeability of the core approaches unity, drastically reducing the transformer inductances, and partially decoupling the primary and secondary circuits. Thus, energy transfer from the primary side to the secondary side essentially stops. Saturation is generally an undesirable effect in transformers.

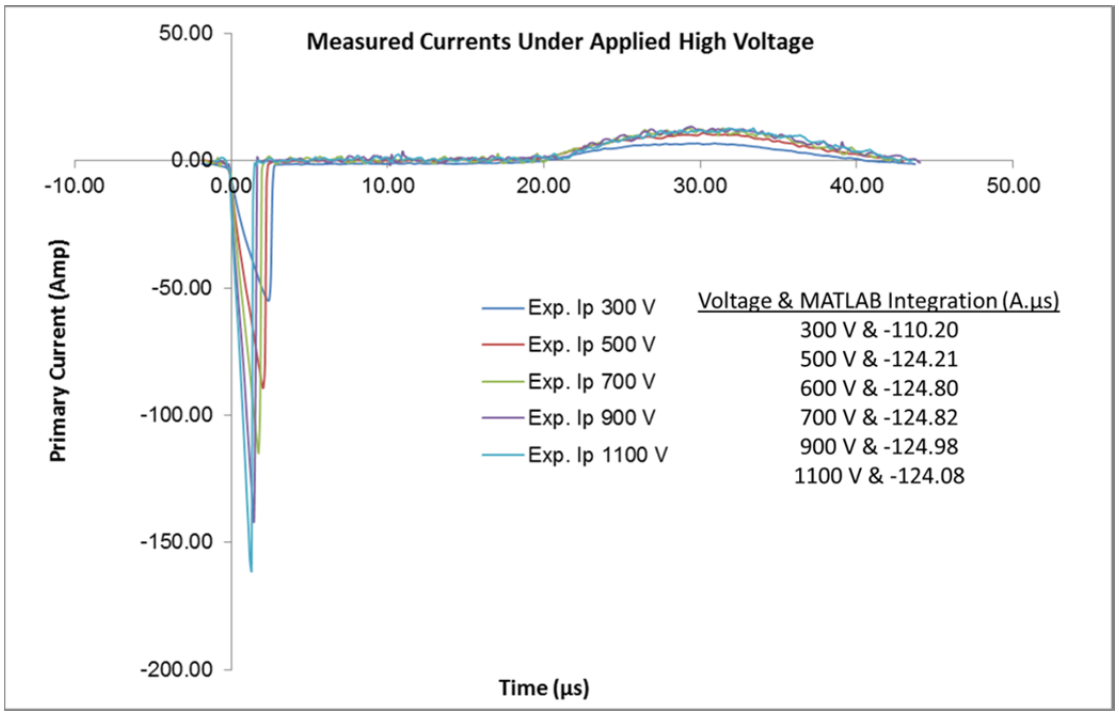

Figure 37. Measured currents under applied high voltage

Figure 37 shows a series of measured primary currents for applied high voltages along with a table listing the charging voltages and corresponding areas under the first part of the current traces. Integration was performed with the "trapezoidal" integration rule using the MATLAB function, . As seen in Figure 37, as the applied charging voltage is increased beyond about 500 V, the area under the curves does not change, which supports the hypothesis of a transformer saturation effect in the pulser.

4. Mitigation Strategies for the Saturation Effect

Saturation of the transformer core inside the pulser was initially thought to be the cause of the distorted current traces during pulser operation at higher charging voltages. Since the transformer consists of a ferrite core, resetting the core could solve the problem. Core reset is a process in which a DC current is applied to the core material in order to mitigate the saturation effect. Various currents in ranging from 0.5 A to 11.5 A were applied to the transformer core; however, no change in scope current trace was observed.

Another hypothesis was that the Bergoz coil, which also contains magnetic core material and measures the primary current, could be the device saturating. To test this hypothesis, a Pearson coil, which is 12.5 times less sensitive (0.1 V/A) than the Bergoz coil (1.25 V/A), was used with the Bergoz coil at the same time in the pulser in order to compare both scope traces.

Figure 38 and Figure 39 demonstrate the primary current measured with the Pearson and Bergoz current transformers, showing good agreement between the Pearson measurement and the theoretical prediction, and saturation only occurring in the Bergoz trace. Therefore, it was the Bergoz coil's core, not the main transformer core, which was saturating.

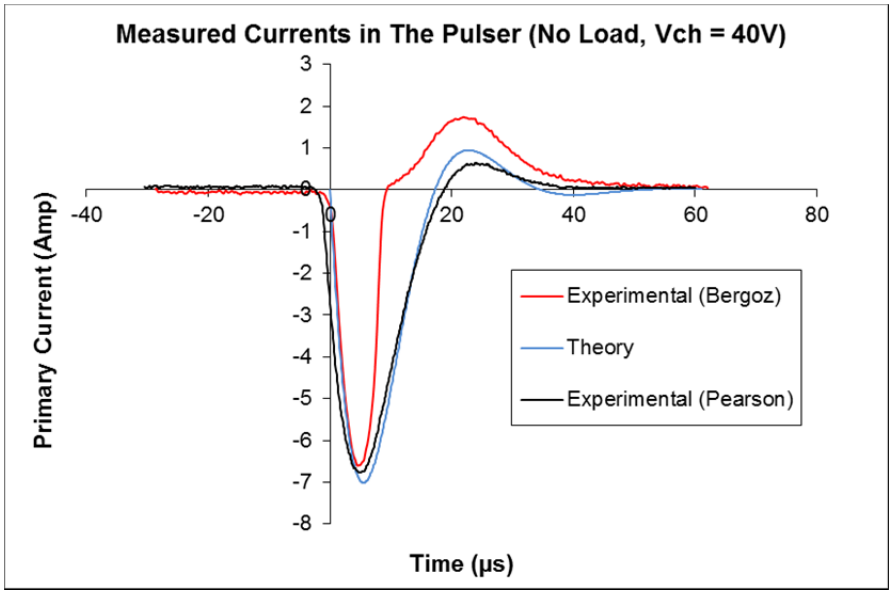

Figure 38. Bergoz coil and Pearson coil scope traces under 40 V

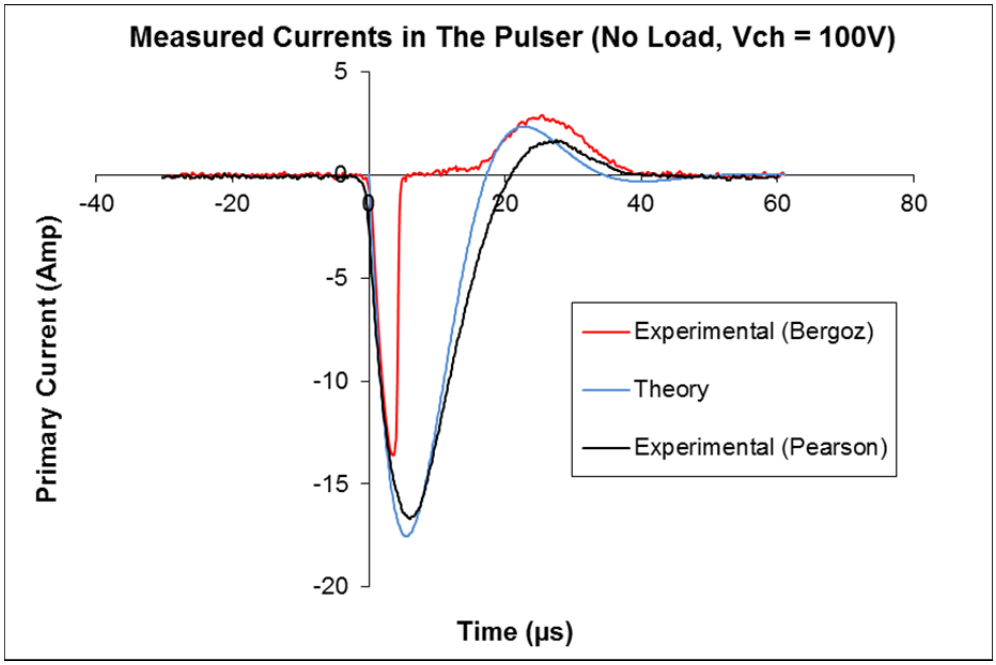

Figure 39. Bergoz coil and Pearson coil scope traces under 100 V

B. VOLTAGE-CURRENT MONITOR

1. General Operation and Design Modifications

The Voltage-Current (V-I) Monitor Box is used for analyzing either loads connected directly to the pulser or a FBPC located inside the vacuum chamber, and provides a flexible tool for measuring the power that the pulser conveys to the FBPC. Because of the location of the FBPC inside the vacuum chamber, the V-I Monitor Box puts the diagnostics as close to the FBPC as possible while still allowing replacement of parts such as resistor loads and Bergoz coils without any interruption of the FBPC operation in the vacuum.

Figure 40 illustrates the V-I Monitor Box circuit diagram inside the red border. The transformer before the V-I Monitor Box is the last element of the pulser. The pulser is connected to the box directly by coaxial cable. The box is connected to the FBPC inside the vacuum chamber. The secondary side current of the transformer as drawn in Figure 40 occurs when only the load is connected

to the pulser, while the secondary current is shared between the load and the spark gap when the FBPC is connected to the box.

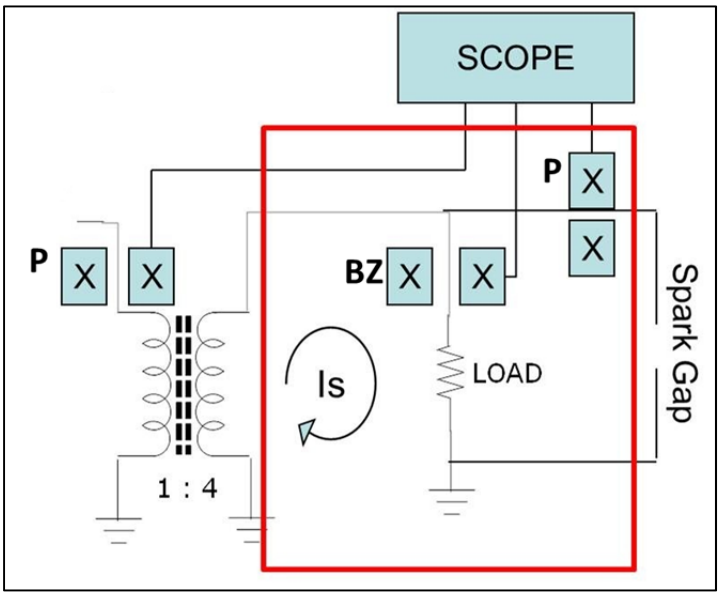

Figure 40. V-I Monitor Box circuit diagram (inside the red border). Location of Bergoz (BZ) and Pearson (P) current monitors shown.

Instead of Pearson coils (Model No: 110 and 411, output volts per amp: 0.1) as drawn in Figure 40, Bergoz coils were originally used for I_p and I_{fb} (flashboard current) measurements before the saturation effect was understood. The Bergoz coil used to monitor V_{fb} (flashboard voltage) was retained, with the load resistance increased to prevent it from going into saturation.

2. Voltage and Current Monitoring

Voltage and current monitoring is the main function of the V-I Monitor Box. The first idea behind this design is to measure voltage by using a current monitor across the load, which has the same voltage applied to it as the FBPC since they are in parallel. The second idea is to measure the current through the FBPC by using another current monitor in series with it as shown in Figure 40. To verify the proper operation of the V-I Monitor Box, one test is to operate it under “open circuit” conditions, without a FBPC attached.

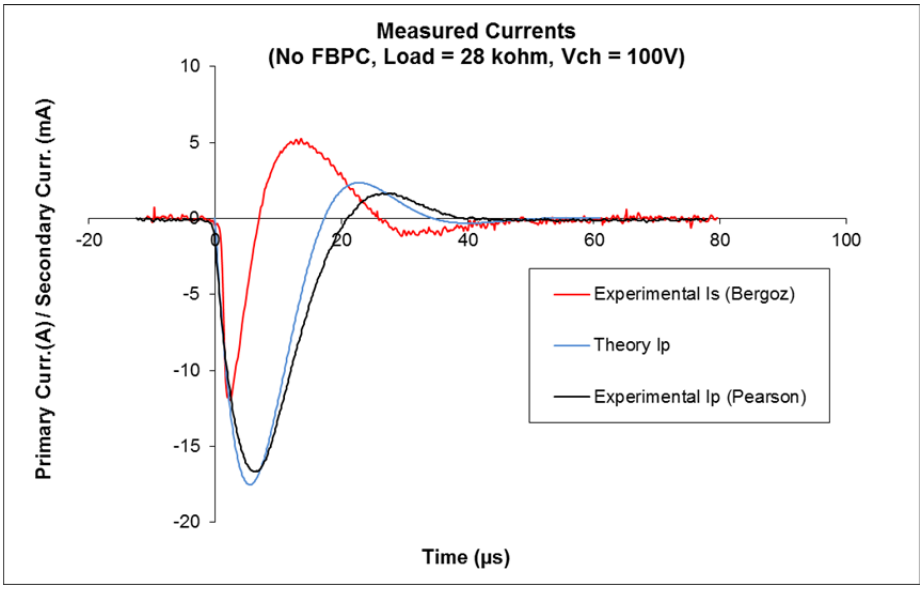

Figure 41. Measured currents with a simple 28 kΩ load in V-I Monitor Box, and with 100 V pulser operation voltage (no FBPC in this part of the experiment)

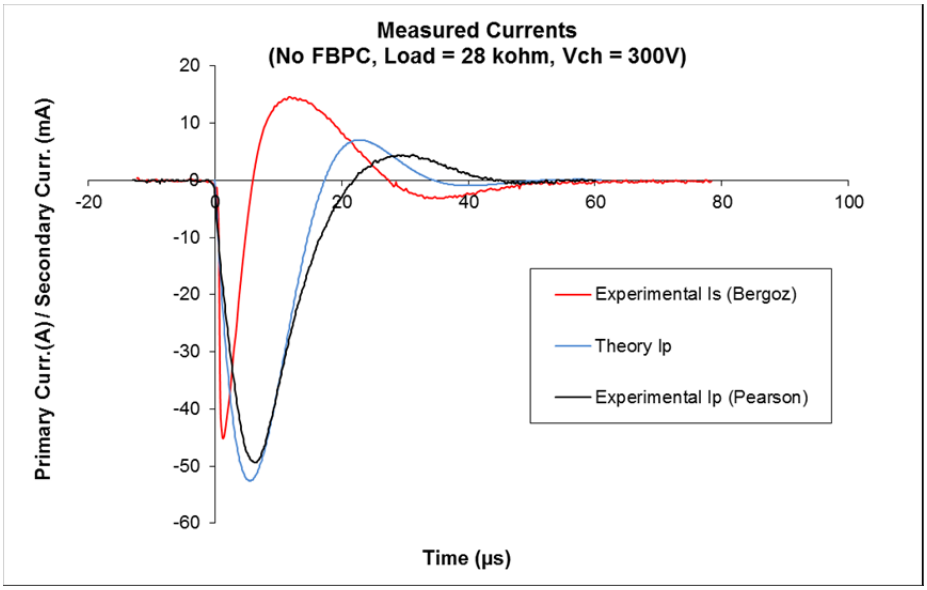

Figure 42. Measured currents with a simple 28 kΩ load in V-I Monitor Box, and with 300 V pulser operation voltage (no FBPC in this part of the experiment)

Figure 41 and Figure 42 represent experimental results of the V-I Monitor Box and the pulser current measurements under low and high charging voltages with a 28 kΩ load, connected to the secondary side of the transformer.

C. FLASHBOARD BREAKDOWN AND PLASMA GENERATION

1. Flashboard Breakdown

With the pulser assembled and connected to the surrogate flashboard through the V-I Monitor Box, the system is ready to generate plasma. The capacitor is charged, and then discharged on command through the SCR, providing a pulse to the primary side of the transformer, which steps up the voltage by a factor of four and steps down the current by a factor of four in preparation for being sent to the flashboard. At this point, the only visual indication that the system has fired is a bright spark over the gap between the electrodes on the flashboard. The brightness of the spark changes in proportion to the pulser charging voltage.

The breakdown process is very complicated and there are competing theories to explain it. One widely held theory is the secondary electron emission avalanche model, in which applied high voltage leads to a prebreakdown avalanche of secondary emission electrons across the dielectric surface. This causes electron-stimulated desorption of gas from the surface, and that gas is then ionized by the electron avalanche to form the surface flashover plasma [38].

For the purposes of this research, the real question at this stage should be: “What is happening electrically right at the time of breakdown of the flashboard?” In order to understand this, understanding the voltage and current behavior during the breakdown is significant, and may lead to a better understanding of the relationship between the power applied to the plasma and its properties, like expansion speed, that affect emittance.

In order to break down the FBPC, pulser charging voltage was fixed to 500 V. Figure 43 shows the behavior of measured currents in the pulser and in the V-I monitor box before the FBPC was attached.

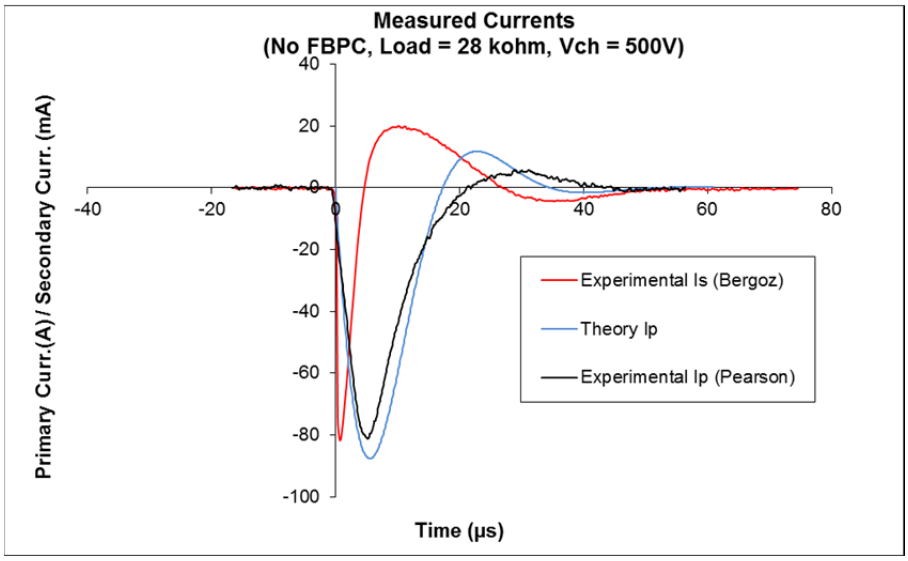

Figure 43. Measured currents under applied 500 V operational pulser voltage before the FBPC is attached to the circuit

After the FBPC is attached to the circuit, red scope trace in Figure 44 illustrates the FBPC current trace measured with the Pearson coil in series with the FBPC.

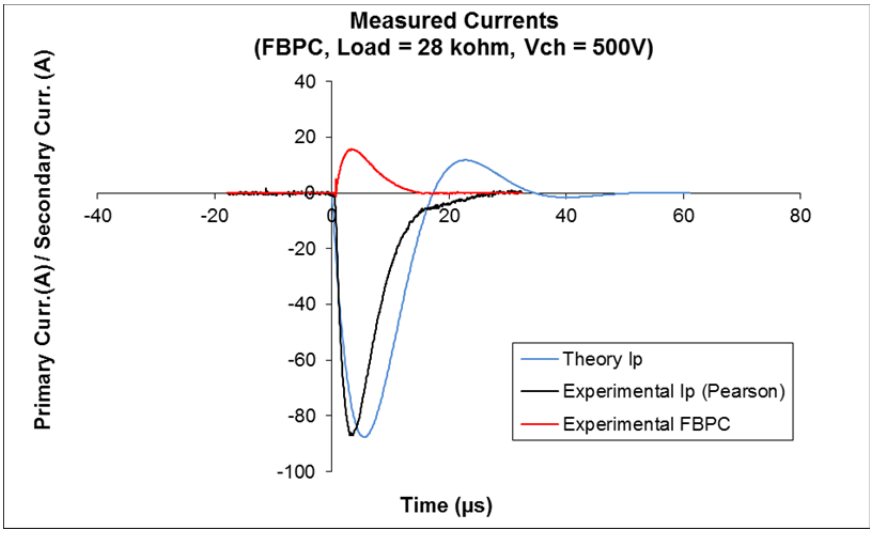

Figure 44. Measured currents under applied 500 V operational pulser voltage after the FBPC is attached to the circuit

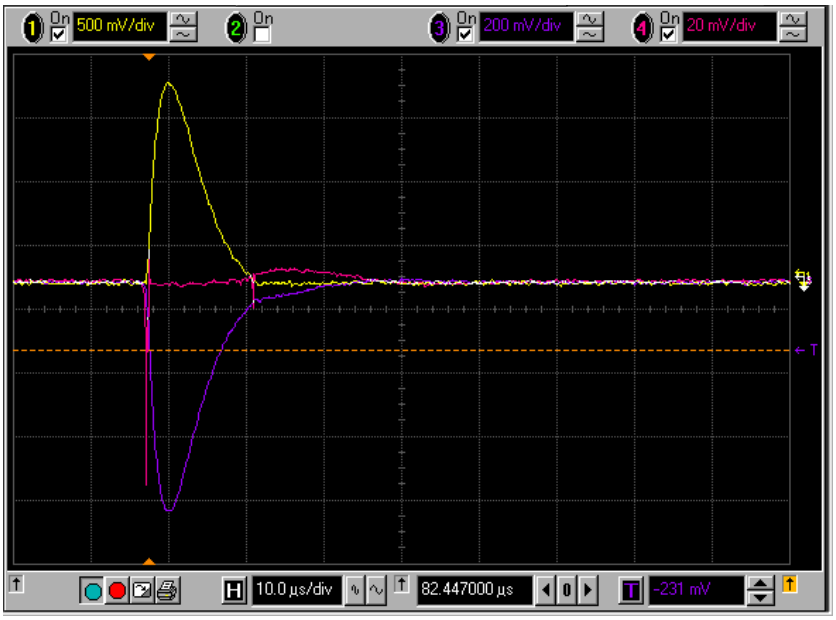

Figure 45. FBPC voltage trace (pink), current trace (yellow), 10x reduced pulser primary current trace (violet) under applied 500 V charging voltage

In Figure 45, while the pink trace represents the FBPC voltage trace, as determined from the Bergoz coil measurement across the load, the yellow trace is the FBPC current trace, measured with the Pearson coil in series with the flashboard as shown in Figure 40. Figure 46 is a detail of the first 500 ns period of the breakdown process; notice that the vertical scale has changed. Also note the current and voltage oscillations that precede the main breakdown and FBPC current pulse.

Figure 46. First 500 ns period of the break-down process shown by FBPC voltage trace (pink), current trace (yellow), pulser operational current trace (violet) under applied 500 V charging voltage

2. Plasma Generation

Plasma generation occurs after the flashboard breaks down under the applied high voltage. In this experiment, the first two goals are to verify that plasma is present, and then to determine how it moves. In this test stand, the plasma cannot be seen by the naked eye as it moves away from the discharge site. Instead, a Langmuir probe can be used as a movable charge collector to verify the plasma's presence and to analyze its motion.

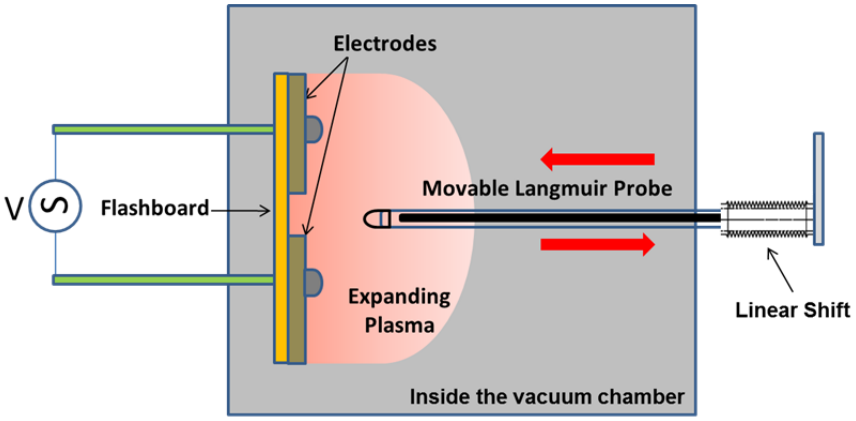

Figure 47. Plasma recognition by using Langmuir probe inside the vacuum chamber after flashboard breaks down

Figure 47 demonstrates how a Langmuir probe is used in order to recognize plasma that exists after the flashboard breaks down. The Langmuir probe is immersed in the region of expected plasma at a distance of one or two inches away from the flashboard. When the plasma reaches the probe tip, charge is deposited on the tip, generating a current through the resistor shown in Figure 26, which is detected as a current on the oscilloscope.

3. Use of Langmuir Probe and Time Delay

The movement of plasma in a vacuum chamber can also be studied experimentally by using this test stand. Since the plasma expands after it is generated, the Langmuir probe can be used to measure the time delay between when the plasma is formed and when it reaches the probe at some known distance from the flashboard. This time of flight measurement would give an estimate for the plasma expansion velocity. However, it would only give that velocity averaged over a specific distance, and would require careful calibration of the experiment (for example, cable delays), to prevent the introduction of errors. Instead, a movable probe is used, and the change in arrival time of the plasma is investigated as the probe's location is changed. Figure 48 illustrates how the probe can be used in this way. When the probe is moved by a distance Δx, the arrival time of the plasma is delayed by a time Δt. Repeating this

measurement at different locations builds up a curve, and the slope of that curve gives a measurement of the plasma's instantaneous velocity as a function of distance away from the FBPC. In principle, this measurement is self-calibrating – as long as the pulser and flashboard behave exactly the same on each shot. There is no need to know exactly when the flashboard breaks down. However, it does require many shots, and shot-to-shot variations in flashboard and pulser operation are an important source of error in this technique.

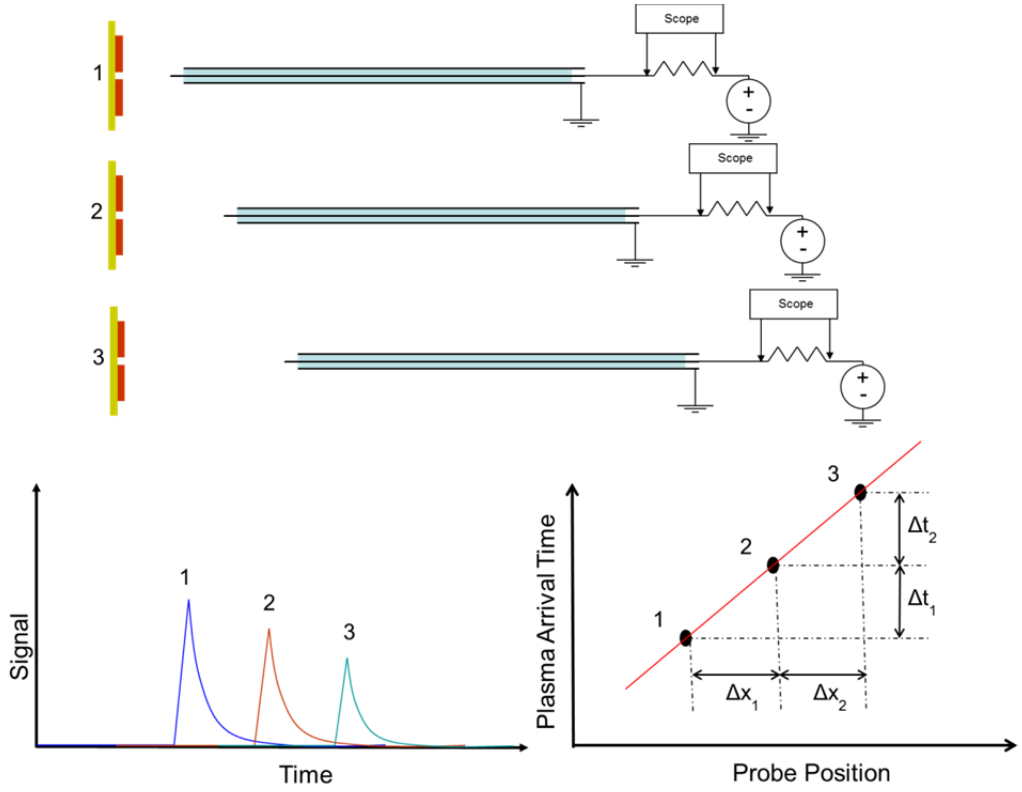

Figure 48. One way of using the Langmuir probe to measure plasma velocity (From [13])

Figure 48 simplifies the idea of understanding the plasma movement. However, it is not as simple as seen in Figure 48 since the shape of the plasma signal on the probe is not a smooth line as shown there. Instead, the plasma signal oscillates and dies down while time passes. Thus, it is sometimes hard to choose a single point along the pulse that clearly defines the arrival of plasma at

the probe. Second, the time of plasma formation is unknown. Therefore, a starting point or reference time must be defined to measure the time when plasma reaches the Langmuir probe. This reference time is the point on the FBPC current signal where this signal begins to appear as shown in Figure 49.

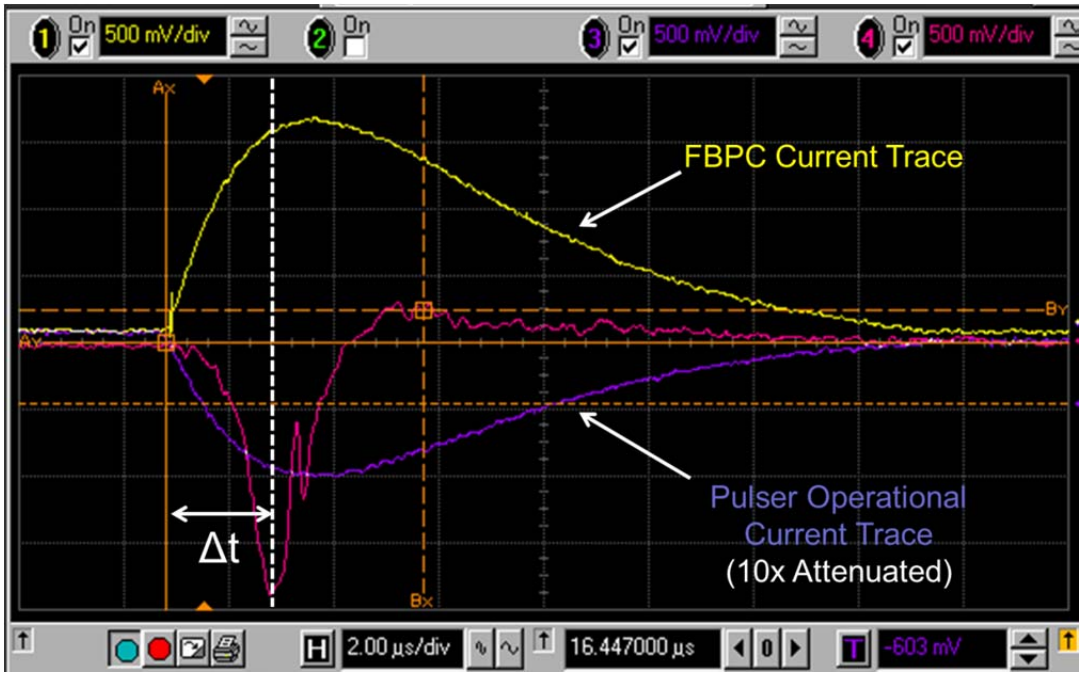

Figure 49. Typical measurement of pulse arrival time to the Langmuir probe

Figure 49 demonstrates a typical measurement made with the new Langmuir probe design shown in Figure 25. In this case, the pulser charging voltage is equal to 500 V and the Langmuir probe is one inch away from the flashboard. To measure the time delay of plasma movement in the vacuum gap, the time difference between the beginning of the current signal measured using the V-I Monitor Box and the highest point of the probe signal (pink trace) are used as shown in Figure 49. This is repeated four times at the first probe position, and then the probe is moved to a new location and the measurements repeated.

The Langmuir probe distance versus time delay data based on this measurement method is plotted in Figure 50, again for a 500 V charging voltage.

A linear fit to the data from the first shot in each location is also shown. The inverse of the slope of this line gives the instantaneous velocity, which is approximately 2.13 cm/μs under the applied 500 V charging voltage. The good agreement with a linear fit indicates that the plasma is expanding ballistically, without accelerating or decelerating, as expected.

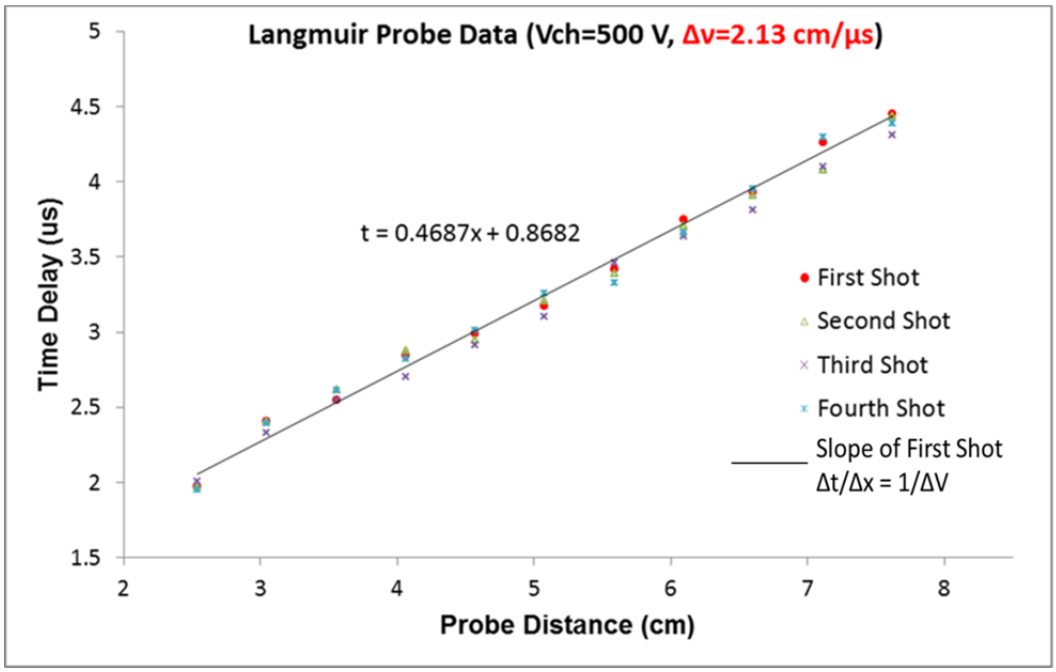

Figure 50. Time delay of Plasma

Three scope traces shown in Figure 51 demonstrate how the plasma signal (pink trace) is affected in amplitude and delay time when the distance of the probe from the FBPC changes; note the change in vertical scale of the pink trace.

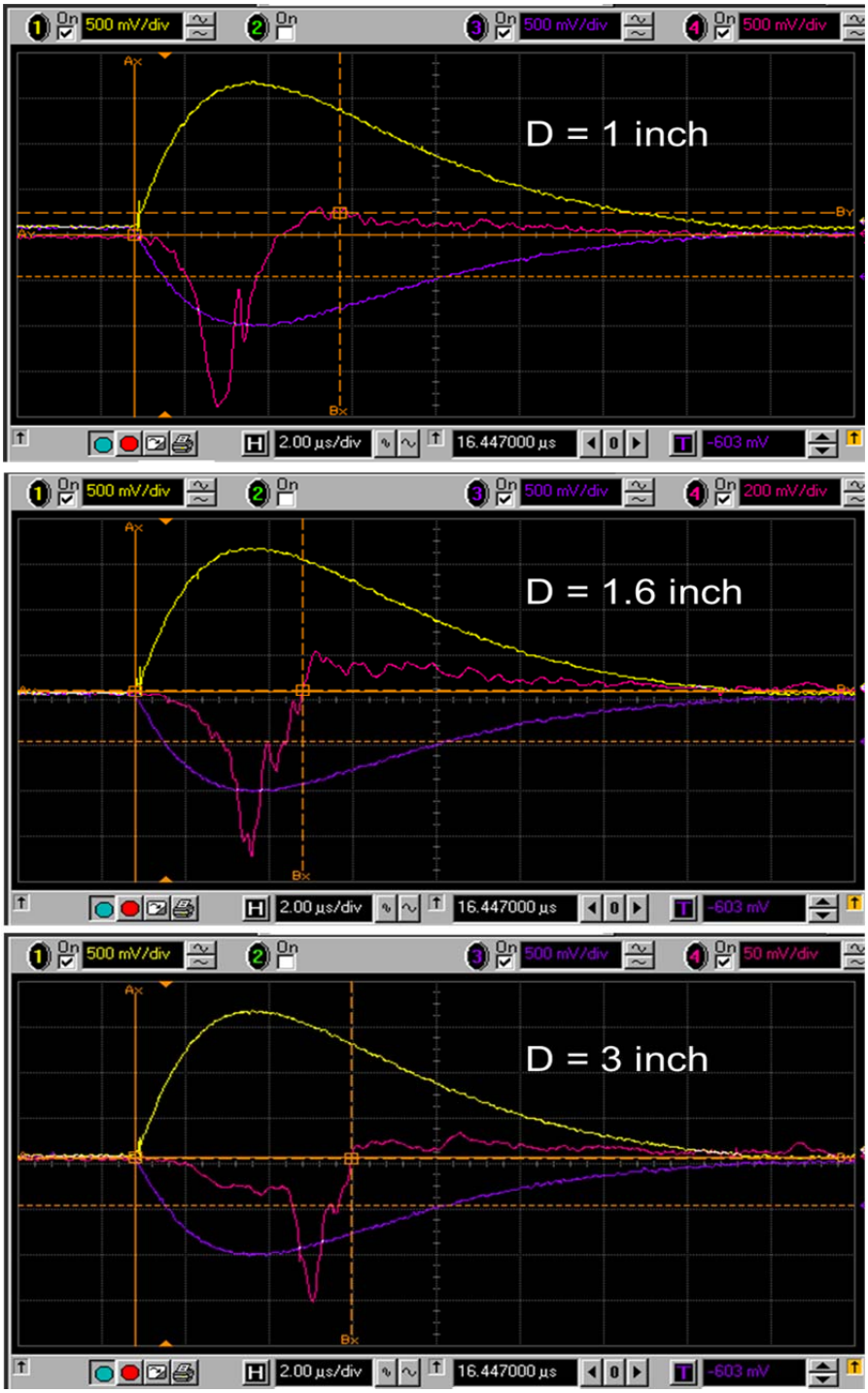

Figure 51. Distance effect on the plasma time delay. The pink trace is the Langmuir probe plasma signal, the yellow trace is the current of the FBPC, and the violet trace is the 10x reduced primary current.

IV. CONCLUSION AND FUTURE WORK

A. SUMMARY

With examination and experimentation, unique ideas may prove that everything can exist in our real world. Reaching for a yet unknown phenomenon occurs when the thinking process begins. Thinking of how to find something that may be imagined, but is not yet known, was the first step of this research. The process involved thinking about the idea, reinforced by reading, and further learning. Then, the sharing of ideas and thoughts further increased the knowledge. Finally, enthusiasm enabled the building of the FBPC test stand and the running of experiments with the goal of benefit for today's and future militaries.

This project has focused on building a test stand to understand how flashboards operate and to see what can be discovered by experimenting with FBPC operation, with the goal of improving them for use in HPMWs.

First, flashboard operation was investigated by designing and building a surrogate flashboard with only one pair of electrodes to simulate an actual flashboard with an array of electrodes. This design facilitated the work and illustrated, in detail, the process of how a real flashboard operates. Designing this flashboard was straightforward and inexpensive because it requires simple dielectric and conducting materials such as aluminum and plastic. In addition to that, it is a simple, rugged design. During all experimental operations, the surrogate flashboard worked without need for any replacement. No contamination of cathode material was detected at all.

Second, one of the major requirements of an FBPC test stand was a pulsed power system. In order to achieve this, a pulser that generates a single pulse with a pulse length of approximately 20 μs, enough to break down the flashboard, was built. Shorter pulses helped in understanding the operation of the flashboard on nanosecond scales.

Third, a Langmuir probe, just a wire in its simplest design, was used to good effect in the test stand. It helped in collecting data about the plasma formation after the flashboard breaks down, as well as the plasma movement through the vacuum gap by taking measurements at different distances from the flashboard.

Fourth, provision was made for the selective measurement of electrons and positive ions in the flashboard plasma. This was achieved by using a grid mechanism, called the “ion stopper” and different power supplies in the test stand. The grid mechanism generates an electric field in the area between the Langmuir probe and the grid, allowing either the positive particles or the negative particles in the plasma to be selected depending on the bias voltage applied to the Langmuir probe.

Fifth, vacuum systems are another aspect of the FBPC test stand. The operation of the test stand does not require an ideal vacuum; however, it needs to run under vacuum in order to mitigate air ionization by the high voltage pulse, and to allow free motion of the plasma. This FBPC test stand has run at modest vacuum levels such as 10^{-7} Torr. This level of vacuum pressure was reached by using a turbomolecular pump and an ion pump.

B. FUTURE WORK

Suggested future tests to be conducted and improvements to be added to the current FBPC test stand include:

- A new pulser generating shorter pulses may increase the effectiveness of the test stand.
- Designing different flashboards and trying different electrode configurations may provide better understanding of the breakdown process.

- Adding an anode plate as shown in Figure 52 should be tested without using an “ion stopper grid” and the results should be compared to the ones acquired by using the ion stopper. This anode plate may well decouple the plasma generation process from the pulse formation.

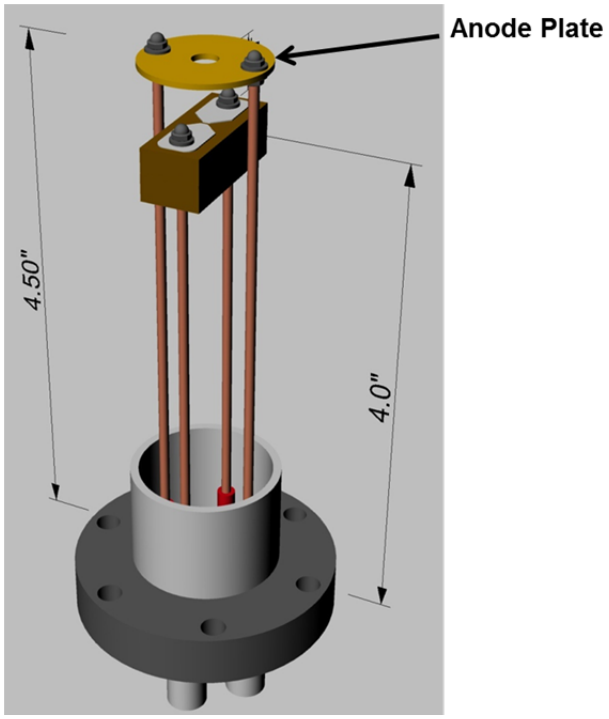

Figure 52. Future design of FBPC with anode grid

- Using multiple Langmuir probes as illustrated in Figure 53. Taking measurements at the same time from different locations can result in much more valuable data about the shape and the content of the plasma and the pulsed electron beam.

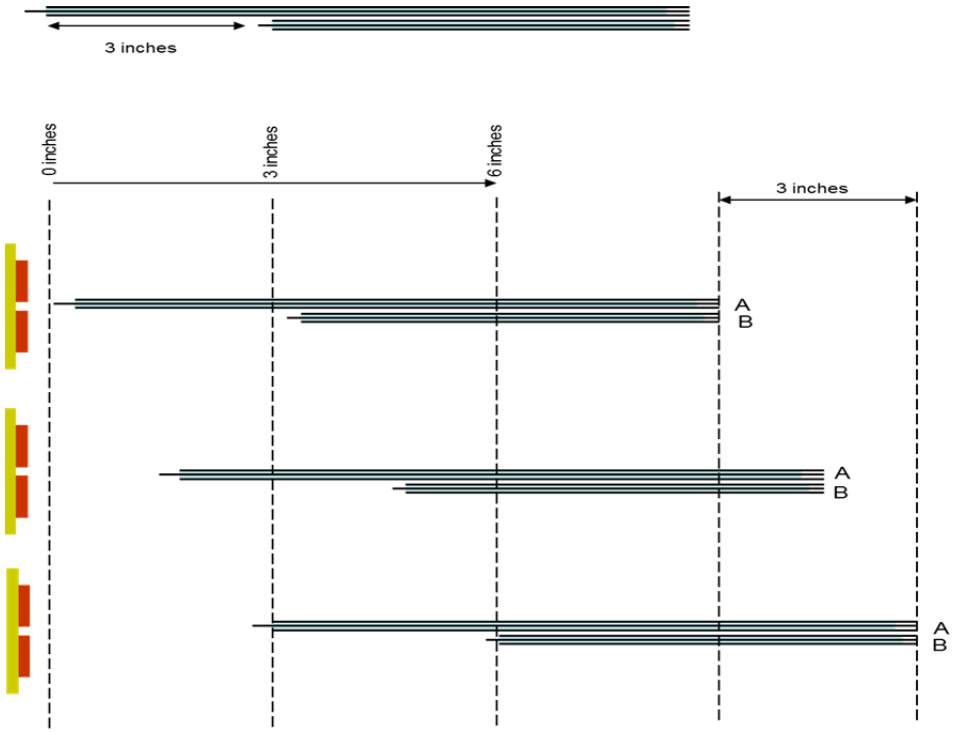

Figure 53. Prospective use of multiple Langmuir probes in future experiments (From [13])

- This test stand has been designed to operate under a maximum 1.2 kV DC source and generates a maximum 5 kV potential. Higher voltages than these maximum levels may improve the effectiveness of the test stand, and should be tested. A new pulser will be required for this operation.

LIST OF REFERENCES

[1] Th.H.G.G. Weise, M.Jung, D. Langhans, M. Gowin, "Overview of directed energy weapon developments," *in 12th Sp. on Electromagnetic Launch Technology 2004,* 25–28 May 2005, pp. 483–489.

[2] E. Van Keuren, Dr.J. Knighten, "Use of high power microwave weapons," *in Institute of Electrical and Electronics Engineers 29th Annual 1995 International Carnahan Conf. on Security Technology 1995,* 18–20 Oct 1995, pp. 482–491.

[3] M. Abrams, "Dawn of the E-bomb," *in IEEE Spectrum,* vol. 40, no. 11, pp. 24–30, Nov. 2003.

[4] E. M. Oks, "Physics and technique of plasma electron sources," *Plasma Sources Sci. Technol.,* vol. 1, no. 4, pp. 249–255, Nov. 1992.

[5] Guoqi Ni, Benqing Gao, Junwei Lu, "Research on high power microwave weapons," *in Proc. Asia-Pacific Microwave Conf.,* 2005.

[6] H. Keith Florig, "The future battlefield: A blast of gigawatts?" *in IEEE Spectrum,* vol. 25, no. 3, pp. 50–54, Mar. 1988.

[7] J.J.A. van der Burgt, P.van Gelder, "Pulsed power requirements for future naval ships," *in 12th IEEE International Pulsed Power Conf., 1999,* vol. 2, pp. 1357–1360.

[8] S. E. Sampayan, S. H. Gurbaxani, and M. T. Buttram, "Plasma-cathode-initiated vacuum gap closure," *J. Appl. Phys.,* vol. 68, no. 5, pp. 2058–2062, Sep. 1990.

[9] A.W. Cross and A.D.R. Phelps, "Progress in pulsed high power microwave source research at the university of strathcly," *in 25th International Conf. on Infrared and Milimeter Waves,* 2000, pp. 379–380.

[10] S.T. Thornton, A. Rex., *Modern Physics for Scientists and Engineers, 3rd Ed. Thompson, Brooks/Cole,* 2006, pp.103–105.

[11] Thermionic Emission in an Electron Gun, [Online]. Available: *http://fizzika.blogspot.com/* [accessed 07 Jan 2012].

[12] University of Virginia, Department of Astronomy. [Online]. Available: http://www.astro.virginia.edu/class/oconnell/astr1230/im/photoelectric-effect-2.jpg [accessed 07Jan 2012].

[13] J.R. Harris, e-mail message to author, 31 Jul 2011.

[14] Electron Emission, [Online]. Available: http://www.oocities.org/tube_theory/ElectronEmission.htm [accessed 07 Jan 2012].

[15] Andrew Hayes Monica, “In-plane carbon nanotube field emitters for high temperature integrated electronics,” Ph.D. dissertation, Georgetown University, 2008. [Online]. Available: http://www.grin.com/en/doc/257862/in-plane-carbon-nanotube-field-emitters-for-high-temperature-integrated [accessed 07 Jan 2012].

[16] Arrays of Fibers, [Online], Available: http://other.nrl.navy.mil/CREBWorkShop/Knowles.pdf [accessed 19 Mar 2012].

[17] John Walter, John Mankowski, and James Dickens, “Imaging of the explosive emission cathode plasma in a Vircator high power microwave source,” *IEEE Trans. on Plasma Sci.,* vol. 36, no. 4, pp. 1388–1389, Aug. 2008.

[18] J.R. Harris, B. Hickman, R. Anaya, E.G. Cook, S. Hawkins, C. Holmes, J. Stanley, J. Watson, G. Caporaso, “Plasma cathode for a short-pulse dielectric wall accelerator,” *IEEE Trans. on Plasma Sci.,* vol. 37, no. 6, pp. 1069–1077, Jun 2009.

[19] S. Humphries, M. Savage, and D. M. Woodall, “High current density plasma cathode,” *Appl. Phys. Lett.,* vol. 47, no. 5, pp. 468–470, Sep. 1985.

[20] T. Letardi, P. Di Lazzaro, G. Giordano, and C. E. Zheng, “Large area X-ray preionizer for electric discharge lasers,” *Appl. Phys. B.,* vol. 48, no. 1, pp. 55–58, 1989.

[21] S. Humphries, J. J. Ramirez, and M. G. Wilde, “Large area pulsed electron sources,” *IEEE Trans. Plasma Sci.,* vol. PS-8, no. 4, pp. 517–519, Dec 1980.

[22] J. J. Ramirez and D. L. Cook, “A study of low-current-density microsecond electron beam diodes,” *J. Appl. Phys.,* vol. 51, no. 9, pp. 4602–4611, Sep. 1980.

[23] T. J. Renk, “Flashboards as a plasma source for plasma opening switch applications,” *J. Appl. Phys.,* vol. 65, no. 7, pp. 2652–2663, Apr. 1989.

[24] D. Colombant, B. Weber, “A simple model for flashboard plasma expansion,” *IEEE Trans. on Plasma Sci.,* vol. ps-15, no. 6, pp. 741–746, Dec 1987.

[25] J. Thompson, D. Husovsky, A. R. Miller, K. Robertson, R. Ingermanson, and D. Parks, “Flashboard plasma source characterization for microsecond plasma opening switches,” *in Proc. 9th Pulsed Power Conf., Dig. Tech. Papers, vol. 1, pp. 524–527, 1993.*

[26] M. D. McFarland, A. Bixier, M. Krishnan, and D. Huet, “Density measurements in flash board plasmas for a magnetically confined plasma opening switch,” *in Pulsed Power Plasma Sci. IEEE Conf. Rec.—Abstracts,* 2001, p. 587.

[27] J. P. Lidestri and R. J. Kares, “Plasma source characterization and development for the density controlled opening switch,” *in Proc. 7th Pulsed Power Conf.,* 1989, pp. 262–267.

[28] B. V. Weber, D. D. Hinshelwood, and R. J. Commisso, “Interferometry of flashboard and cable-gun plasma opening switches on hawk,” *IEEE Trans. Plasma Sci.,* vol. 25, no. 2, pp. 189–195, Apr. 1997.

[29] C. Grabowski, J.M. Gahl, and E. Schamiloglu, “A cathode mounted plasma prefill source for high power microwave experiments,” *in 11th IEEE International Pulsed Power Conf.,* 1997, vol. 1, pp. 747–752.

[30] R. Arad, K. Tsigutkin, Y. V. Ralchenko, and Y. Maron, “Spectroscopic investigations of a dielectric-surface-discharge plasma source,” *Phys. Plasmas,* vol. 7, no. 9, pp. 3797–3807, Sep. 2000.

[31] S. Humpries, S. Coffey, M. Savage, L.K. Len, G.W. Cooper, “Grid-controlled plasma cathodes,*” J. Appl. Phys.,* vol. 57, no. 3, pp. 709–713, Feb 1985.

[32] J.R. Bayless, R.C. Knechtli, G.N. Mercer, “The plasma-cathode electron gun,” *IEEE Journal of Quantum Electronics,* vol. 10, no. 2, pp. 213–218, Feb 1974.

[33] Ady Hershcovitch, “Extraction of superthermal electrons in a high current, low emittance, steady state electron gun with a plasma cathode,” *Appl. Phys. Lett.,* vol. 68, no 4, pp. 464–466, Jan. 1996.

[34] E. M. Oks and P. M. Schanin, “Development of plasma cathode electron guns,” Phys. Plasmas, vol. 6, no. 5, pp. 1649–1654, May. 1999.

[35] W. A. Barletta, J. K. Boyd, A. C. Paul, and D. S. Prono, “Brightness limitations in multi-kiloampere electron beam sources,” *presented at the Free-Electron Laser Conf.,* Castelgandolfo, Italy, Sep. 3–7, 1984. UCRL-90914. [Online]. Available: https://e-reports-ext.llnl.gov/pdf/196738.pdf

[36] Fast Current Transformer User Manual, [Online], Available: http://www.bergoz.com/manual [accessed 12 May 2012].

[37] Linear Shifts, [Online], Available: http://www.lesker.com/newweb/sample_manipulation/linearmotion_introduction.cfm?pgid=0 [accessed 18 Mar 2012].

[38] R. A. Anderson and J. P. Brainard, “Mechanism of pulsed surface flashover involving electron-stimulated desorption,” *J. Appl. Phys.,* vol. 51, no. 3, pp. 1414–1421, Mar. 1980.

INITIAL DISTRIBUTION LIST

1. Defense Technical Information Center
   Ft. Belvoir, Virginia

2. Dudley Knox Library
   Naval Postgraduate School
   Monterey, California